bioRxiv preprint doi: https://doi.org/10.1101/2020.07.06.190330; this version posted July 6, 2020. The copyright holder for this preprint (which was not certified by peer review) is the author/funder. All rights reserved. No reuse allowed without permission.

Title:

Inflammation Drives Alternative First Exon usage to Regulate Immune Genes including a Novel Iron Regulated Isoform of Aim2

Elektra K. Robinson[1*], Pratibha Jagannatha[1,2*], Sergio Covarrubias[1], Matthew Cattle[2], Rojin Safavi[2], Ran Song[3], Kasthuribai Viswanathan[3], Barbara Shapleigh[1], Robin Abu-Shumays[2], Miten Jain[2], Suzanne M. Cloonan[4], Edward Wakeland[3], Mark Akeson[2], Angela N. Brooks[2#] and Susan Carpenter[1#]

[1]Department of Molecular, Cell and Developmental Biology, University of California Santa Cruz, 1156 High St, Santa Cruz, CA 95064

[2]Department of Biomolecular Engineering, University of California Santa Cruz

[3]Department of Immunology, University of Texas Southwestern Medical Center, Dallas, TX, 75390-9093

[4] Division of Pulmonary and Critical Care Medicine, Joan and Sanford I. Weill Department of Medicine, Weill Cornell Medicine, New York, NY 10021 USA

* Authors contributed equally to this work

Corresponding authors: Angela N. Brooks (anbrooks@ucsc.edu) and Susan Carpenter (sucarpen@ucsc.edu)

bioRxiv preprint doi: https://doi.org/10.1101/2020.07.06.190330; this version posted July 6, 2020. The copyright holder for this preprint (which was not certified by peer review) is the author/funder. All rights reserved. No reuse allowed without permission.

Abstract:

Determining the layers of gene regulation within the innate immune response is critical to our understanding of the cellular responses to infection and dysregulation in disease. We identified a conserved mechanism of gene regulation in human and mouse via changes in alternative first exon (AFE) usage following inflammation, resulting in changes to isoform usage. Of these AFE events, we identified 50 unannotated transcription start sites (TSS) in mice using Oxford Nanopore native RNA sequencing, one of which is the cytosolic receptor for dsDNA and known inflammatory inducible gene, *Aim2*. We show that this unannotated AFE isoform of *Aim2* is the predominant isoform transcribed during inflammation and contains an iron-responsive element in its 5′UTR enabling mRNA translation to be regulated by iron levels. This work highlights the importance of examining alternative isoform changes and translational regulation in the innate immune response and uncovers novel regulatory mechanisms of *Aim2*.

Summary Sentence:

Alternative first exon usage was the major splicing event observed in macrophages during inflammation, which resulted in the elucidation of a novel isoform and iron mediated regulatory mechanism of the protein coding gene, *Aim2*.

Keywords:

Innate Immunity, Macrophages, Alternative Splicing, Aim2, 5’UTR, Nanopore Sequencing

bioRxiv preprint doi: https://doi.org/10.1101/2020.07.06.190330; this version posted July 6, 2020. The copyright holder for this preprint (which was not certified by peer review) is the author/funder. All rights reserved. No reuse allowed without permission.

Introduction:

Macrophages are critical cells in the innate immune system that combat infection by initiating acute inflammatory responses. Acute inflammation is tightly coordinated and begins with the detection of pathogen-associated molecular patterns (PAMPs) by pattern recognition receptors (PRRs), which include Toll-Like Receptors (TLRs) (*1*, *2*). These initial steps are followed by the activation of sequestered transcription factors, such as nuclear factor of kappa-B (NF-kB) and interferon regulatory factors (IRFs), which orchestrate pro-inflammatory and/or antiviral response signals involved in pathogen clearance (*2*). Once pathogens are cleared, macrophages express genes involved in the resolution of inflammation to return the host to homeostasis (*3*). Dysregulation of these pro-inflammatory pathways can have devastating consequences, leading to unresolved inflammation and chronic inflammatory diseases (*4*).

Recently the process of alternative splicing has emerged as another key mechanism by which the immune system is regulated. Alternative splicing is a regulated process enabling a single gene to produce many isoforms, thus increasing the complexity of gene function and the proteome (*2*, *5–7*). Much of this occurs in a cell-type-specific and signal-induced manner (*8*, *9*). Previous studies have shown that mouse and human macrophages exposed to inflammatory stimuli undergo alternative splicing (*2*, *10–18*). Alternative splicing within the immune system can affect the type and magnitude of the inflammatory response, such as the production of a soluble form of TLR4 that is expressed upon LPS, which leads to inhibition of TNFα and NFκB serving as a negative feedback mechanism (*19*, *20*). Additionally, this mechanism has been characterized within signaling molecules (*21*, *22*), including TBK1 (*23*) and MyD88 (*24*), that produce the alternative RNA splice forms, TBK1s and MyD88s respectively, which function to limit the extent of the pro-inflammatory response. Alternative splicing can also result in the production of inflammatory

bioRxiv preprint doi: https://doi.org/10.1101/2020.07.06.190330; this version posted July 6, 2020. The copyright holder for this preprint (which was not certified by peer review) is the author/funder. All rights reserved. No reuse allowed without permission.

signaling molecules, such as TRIF (*25*) and the proteins in the NFκB family(*9*) with altered activity or stability. Beyond changing the ORF of an mRNA molecule, elongating or shortening the first or last exon can impact post-transcriptional gene regulation and are important to consider when elucidating the regulatory mechanisms of immune genes (*26–28*), specifically underlying motifs in 5'UTRs (*29*, *30*) and 3'UTRs (*31*, *32*).

While inflammation-induced alternative splicing in both human and mouse macrophages has been investigated on a genome-wide scale (*2*, *10–18*), to our knowledge, long read RNA-sequencing has not been utilized to investigate differential RNA isoform expression. Such an approach is necessary to fully appreciate the extent of alternative splicing as we know most transcriptome annotations are incomplete (*33*), and isoforms generated are cell-type and treatment specific (*33–36*).

Here we used both long and short-read RNA sequencing to uncover novel isoforms and classes of alternative splicing events following inflammation in human and murine macrophages. Interestingly the dominant conserved class of alternative splicing observed following inflammation is alternative first exon usage (AFE). AFE events can have a multi-level effect on protein diversity, regulating genes through alterations of the 5′UTR region, and directing the locality of proteins through alternative N-termini (*37*). We identified 50 unannotated AFE events in mice from native RNA sequencing, one of which is in the cytosolic receptor for dsDNA and known inflammatory inducible gene, *Aim2*. We show that this unannotated AFE isoform of *Aim2* is the predominant isoform produced during inflammation and contains an iron-responsive element in its 5′UTR, enabling mRNA translation to be controlled by iron levels. This work reveals that alternative splicing plays a crucial role in shaping the transient nature of the inflammatory response. Isoform expression is an additional layer of regulation within the immune response and

bioRxiv preprint doi: https://doi.org/10.1101/2020.07.06.190330; this version posted July 6, 2020. The copyright holder for this preprint (which was not certified by peer review) is the author/funder. All rights reserved. No reuse allowed without permission.

therefore a possible contributing factor to the development of auto-immune and inflammatory diseases. Understanding the exact isoforms of genes that are expressed during an inflammatory response will enable us to design better targets for therapeutic intervention of these diseases.

Results:

Global profiling of the cellular alternative splicing landscape in human and mouse macrophages post-inflammation.

To identify alternative splicing events following inflammation, we performed whole transcriptome analysis on human monocyte derived macrophages (MDMs) and murine bone marrow derived macrophages (BMDMs) with and without lipopolysaccharide (LPS) treatment (Fig. 1A). We found that ~50% of splicing changes (corrected p-value ≤ 0.25 and $|\Delta PSI| \geq 10$) were classified as alternative first exon (AFE) events following LPS activation in both human and murine macrophages (Fig. 1B, SFig. 1). We next identified 12 conserved AFE splicing events between human and mouse (SFig. 2). We validated the AFE changes upon stimulation on the already characterized *Ncoa7* (SFig. 3A-C) (*38*, *39*) and *Rcan1* (SFig. 3D-F) (*40*), as well as a previously uncharacterized inflammatory specific isoform of *Ampd3* (SFig. 3G-I), in human and mouse primary macrophages using RT-PCR. Taken together, these results show the high prevalence and conservation of alternative first exons following inflammatory activation.

A caveat to our analysis thus far was the reliance on annotated transcriptome assemblies. In order to determine if there are additional splicing events that are not captured using short-read sequencing (*33*, *41–43*), we performed native RNA sequencing of murine macrophages with and without LPS treatment. We identified isoforms using Full-Length Alternative Isoform analysis of RNA (FLAIR) (*33*, *44*) that also had promoter support identified from accessible chromatin (ATAC-seq) (*45*, *46*). The FLAIR isoforms were then merged with the GENCODE M18 assembly

bioRxiv preprint doi: https://doi.org/10.1101/2020.07.06.190330; this version posted July 6, 2020. The copyright holder for this preprint (which was not certified by peer review) is the author/funder. All rights reserved. No reuse allowed without permission.

(mm10) (*47*) to identify and quantify alternative splicing events (SFig. 4). Overall, the incorporation of long-read sequencing led to the identification of 50 novel and statistically significant AFE events that occur following inflammation (Fig. 1C-D). Interestingly, when identifying gene expression changes, we found that ~50% of genes with AFE usage were not differentially expressed following inflammation (Fig. 1E-F) (Table 4-5), highlighting the importance of studying isoform usage for control of gene expression. Among the most statistically significant novel AFE first exon events were *Denr*, *Arhgef7,* and *Aim2*, which we validated using RT-qPCR (Fig. 1G-I) (SFig. 5).

Identification of an unannotated promoter for Aim2.

To better understand the potential functional consequence of AFE changes, we further examined the novel first exon event upregulated upon inflammatory activation in *Aim2*. *Aim2* is an interferon-stimulated gene (ISG), localized to the cytosol. *Aim2* is a dsDNA sensor, that upon recognition induces the formation of an inflammasome complex releasing IL1β and IL18 from the cell as a defense mechanism to control infection (*48*). Chromatin Immunoprecipitation (ChIP)-seq for the myeloid pioneering transcription factor PU.1 in primary BMDMs (Fig. 2A-B, top track, in black) (*49*) supported the presence of an additional promoter upstream of the RefSeq canonical isoform for *Aim2* (NM_001013779.2). Predominant isoforms (>=10% of total gene expression in a sample) assembled from native RNA sequencing with FLAIR identified the canonical RefSeq isoform and 5 unannotated isoforms that use the inflammatory activated promoter, revealing a new longer 5′UTR (Fig. 2C). Native RNA sequencing-based quantification provided additional support that the unannotated promoter usage is upregulated upon LPS stimulation. At steady-state, approximately 20% of reads map to *Aim2*'s transcript with the canonical promoter and 65% of reads map to transcripts with the upstream promoter, while following inflammatory activation,

bioRxiv preprint doi: https://doi.org/10.1101/2020.07.06.190330; this version posted July 6, 2020. The copyright holder for this preprint (which was not certified by peer review) is the author/funder. All rights reserved. No reuse allowed without permission.

14% of the reads map to transcripts with the canonical promoter and 81% of reads map to transcripts with the upstream promoter (Fig. 2D). To validate the change in *Aim2* AFE usage upon LPS stimulation, RT-qPCR was performed using exon spanning primers that were either specific to the annotated AFE or the unannotated AFE, in BMDMs (Fig. 2E). The expression profile of the annotated first exon is not induced by LPS stimulation (Fig. 2F), while the unannotated first exon and the CDS of *Aim2* are equally induced by LPS stimulation (Fig. 2G-H). Therefore, these data show that it is the novel isoform of *Aim2* is inflammatory-regulated and not the canonical isoform defined in RefSeq annotation, nor isoforms from the GENCODE annotation.

The novel inflammatory promoter of Aim2 is regulated by IRF3 and p65.

To gain insights into potential regulatory mechanisms controlling the expression of the 100 significant AFE events as well as *Aim2*, we assessed changes in chromatin accessibility during inflammatory activation in BMDMs. Analysis of ATAC-Seq (*46*) revealed differential peaks at the promoter regions for 25% of genes with significant AFE events suggesting that chromatin remodeling is one mechanism driving the expression of the AFE events (Fig. 3A). This mechanism is not what controls isoform usage for *Aim2*. The annotated promoter is accessible in all cells while the novel *Aim2* promoter is specific to myeloid progenitors and monocytes (*46*, *50*) (SFig. 6A). In addition, the accessibility of both the annotated and unannotated promoters remain open despite the cell's inflammatory status (SFig. 6B). Therefore, the expression of the new isoform is not due to chromatin remodeling of either promoter region (SFig. 6C).

Another mechanism that can drive AFE usage is transcription factor binding. We next analyzed ChIP-seq data of two major transcription factors that drive inflammation downstream of LPS, nuclear factor of kappa-B (NFkB, p65) and interferon response factor 3 (IRF3) (*46*). We found that p65 and IRF3 specifically account for another 25% of the AFE events, including the

bioRxiv preprint doi: https://doi.org/10.1101/2020.07.06.190330; this version posted July 6, 2020. The copyright holder for this preprint (which was not certified by peer review) is the author/funder. All rights reserved. No reuse allowed without permission.

novel *Aim2* isoform, which we confirmed using multiple ChIP-seq data sets (Fig. 3A-B, SFig. 7AB). Further bioinformatic analysis of the two promoter regions driving the canonical and noncanonical isoforms of *Aim2* resulted in the identification of 106 individual transcription factor (TF) motifs within the annotated promoter and 121 motifs within the unannotated promoter (Table 8). Of these predicted motifs there were 54 motifs unique to the unannotated promoter (Fig. 3C). DAVID gene ontology (*51*) analysis of TFs specific to the annotated and unannotated promoter regions of *Aim2* confirms that the unannotated promoter is driven by inflammatory specific transcription factors including NF-κB and IRFs (Fig. 3D, E) (Table 9). Use of ATAC-seq and ChIP-seq for specific TFs has enabled us to determine the regulatory mechanisms driving 50% of the AFEs in our data. For the remaining 50%, there could be additional TFs, RNA binding proteins (*19*), or differential RNA stability driving their expression. Further work will be required to fully understand the complex regulation of all AFE events.

Unannotated 5'UTR of Aim2 negatively regulates translation through a single iron responsive element.

The novel inflammatory isoform identified here for *Aim2* acquired a longer 5′ untranslated region (UTR) compared to the canonical isoform (Fig. 4A). Previous studies have shown that longer 5′UTRs can affect the translation of a gene (*29*, *52*). Using a GFP reporter system, the translational efficiency of the unannotated *Aim2* 5′UTR (767bp) was compared to the annotated 5′UTR (489bp) (Fig. 4B). The unannotated 5′UTR showed lowest mean GFP fluorescence units, suggestive of lower translational efficiency, as assessed by flow cytometry 72 hr post transient transfection in 293T cells (Fig. 4C-D), while equal mCherry fluorescence was observed for all co-transfected control constructs (Fig. 4E). To explore the mechanism of how the unannotated 5′UTR results in decreased translational efficiency, we used RegRNA2.0 to predict RNA regulatory

bioRxiv preprint doi: https://doi.org/10.1101/2020.07.06.190330; this version posted July 6, 2020. The copyright holder for this preprint (which was not certified by peer review) is the author/funder. All rights reserved. No reuse allowed without permission.

178 motifs in the 5′UTRs (*53*). We identified a single iron-responsive element (IRE) within the
179 unannotated 5′UTR, while Musashi binding elements (MBE) motifs were identified in both
180 5′UTRs (Fig. 4F) (Table 10). The finding that there are more structured motifs in the unannotated
181 5′UTR is also supported by the RNAfold Vienna package (*54*), which predicts the hairpin structure
182 of the IRE element in the alternative 5′UTR (SFig. 8). Since the IRE motif is unique to the
183 unannotated 5′UTR we hypothesized that this motif is critical in regulating translational efficiency.

184 When cells are at homeostasis, Iron Binding Proteins (IRP1/2) bind to IRE elements located
185 within the 5'UTR (e.g. ferritin) can block translation, while IRE elements in the 3'UTR (e.g.
186 transferrin receptor) can promote translation (*55*, *56*). However, iron repletion results in the
187 inactivation of IRP1/2 (*57*) (Fig. 4G). To experimentally test if the IRE motif within the
188 unannotated 5′UTR acts as a translational repressor, we removed the element using site-directed
189 mutagenesis which led to an increase in GFP expression by ~20% compared to the annotated
190 5′UTR (Fig. 4H-I). Next we exogenously added 100 uM ferric ammonium citrate (FAC) to
191 overload the cells with iron and determined if this can rescue the observed decrease in translational
192 efficiency from our unannotated 5′UTR. Upon FAC administration, the relative GFP expression
193 of the unannotated 5′UTR plasmid increased by ~50%, while mCherry control was unchanged,
194 suggesting that the translational efficiency of the unannotated 5′UTR can be rescued with iron
195 supplementation (Fig. 4J-K). From these results, we conclude that the predicted IRE motif within
196 the unannotated 5′UTR of *Aim2* functions as an IRE to control translation.

197 To test if the IRE motif in the unannotated 5′UTR of *Aim2* acts as a translational regulator
198 endogenously, we performed polysome profiling followed by RT-qPCR on primary BMDMs in
199 the presence and absence of LPS for 18 hr to determine the translational competency of the
200 isoforms of *Aim2* (Fig. 4L-M). The relative distribution of our positive control gene, *Gapdh*, which

bioRxiv preprint doi: https://doi.org/10.1101/2020.07.06.190330; this version posted July 6, 2020. The copyright holder for this preprint (which was not certified by peer review) is the author/funder. All rights reserved. No reuse allowed without permission.

encodes a highly expressed housekeeping protein, is enriched in the high polysome fraction as expected (Fig. 4N). As a negative control, we examined Neat1, a long non-coding RNA (lncRNA) that is not detected in polysomes, nor translated (Fig. 4O). Using isoform-specific primer sets (Fig. 2E) for the annotated and unannotated *Aim2* isoforms, we find that the annotated isoform is enriched in the high polysome fraction during no treatment, while the novel isoform is enriched in the low polysome fraction upon inflammatory stimulation (Fig. 4P). These data show that the unannotated *Aim2* isoform has a lower translational efficiency compared to the canonical form. Finally, to further validate the effect of expression of the unannotated *Aim2* isoform on the level of protein, we performed a time-course LPS stimulation for 72 hr, with and without the treatment of iron (FAC) and measured AIM2 expression by western blot. AIM2 is expressed basally and significantly decreases upon LPS treatment at the 48 hr time point, most likely as a control mechanism to return the pathway to homeostasis and limit the inflammatory stimulation. When FAC is added to cells, AIM2 expression does not decrease at the 48 hr time point suggesting that it is indeed the IRE element that is driving this decrease in AIM2 observed in the wild type cells (Fig. 4Q-R).

Discussion:

While we have come a long way in determining the transcriptomes of immune genes to better understand signaling pathways, very little work has focused on the role that mRNA isoforms play (*2*, *58*, *59*). Over 95% of genes have more than one mRNA transcript due to alternative splicing but the regulatory importance of these splicing events are not fully understood (*60–62*). On a gene-by-gene approach, alternative splicing has been shown to play a role in health and disease by shaping the proteome (*63–65*). Globally, a number of labs have tackled the prevalence of alternative splicing *in vitro* and *in vivo* showing that alternative splicing can affect both the

bioRxiv preprint doi: https://doi.org/10.1101/2020.07.06.190330; this version posted July 6, 2020. The copyright holder for this preprint (which was not certified by peer review) is the author/funder. All rights reserved. No reuse allowed without permission.

nature and duration of inflammation (*10*, *11*, *14*). To date no one has examined conservation of these mechanisms using primary cells or utilized long read sequencing to build the transcriptome *de novo* to obtain a complete understanding of the extent of alternatively expressed isoforms generated following an immune response.

In our study, we demonstrate a conservation of splicing, specifically alternative first exon (AFE) events, in both human and murine macrophages. We found that there are 12 genes that have AFE in both human and mouse macrophages (SFig. 2). Most studies to date have focused on isoform changes linked to genes that are differentially expressed following inflammation and interestingly these 12 genes would have been previously overlooked because many of them are not differentially expressed emphasizing the importance in studying isoform expression in all conditions (Fig. 1E-F). Of the 12 conserved genes, 7 AFE isoforms have been previously studied in some context including: Rps6ka1 (*66*), Ncoa7 (*38*, *39*), Rcan1 (*40*), Wars (*67*, *68*), Arap1 (*69*), Adar (*70*, *71*) and Sgk1 (*72–74*). While this validates our technique, it is important to note that none of these genes had been connected to inflammation and formally shown to be conserved mechanisms of regulation, besides Wars (*67*, *68*). This also highlights our method's ability to accurately identify inflammatory regulated RNA isoforms, in addition to the uncharacterized AFE events of Cept1, Ampd3, Snx10, Elf1 and Tspan4. Furthermore, Snx10 and Elf1, two proteins studied outside the context of inflammation, have been implicated in chronic inflammatory disease and our study may suggest new insights into how alternative splicing could be regulating these genes (*64*, *65*). We further validated Ncoa7, Rcan1 and Ampd3 in human and murine macrophages using RT-PCR (SFig. 3).

To overcome the current limitations of any transcriptome build we used direct RNA nanopore technology on primary murine macrophage nanopore to build our own transcriptome *de*

bioRxiv preprint doi: https://doi.org/10.1101/2020.07.06.190330; this version posted July 6, 2020. The copyright holder for this preprint (which was not certified by peer review) is the author/funder. All rights reserved. No reuse allowed without permission.

novo with the aim of identifying novel full transcriptional isoforms (*33*, *44*). Following this, we identified hundreds of novel isoforms resulting in 50 novel AFE events (Fig. 1), including an unannotated mRNA isoform of the well-studied gene protein absent in melanoma 2 (*Aim2*).

Aim2 is characterized as an interferon inducible gene (*75*) (PMID: 10454530), functioning as a cytoplasmic dsDNA sensor leading to the formation of an inflammasome and eventual cleavage and release of pro-inflammatory cytokines of IL1β and IL18 (*76–78*). Our study highlights that it is an alternative mRNA isoform of Aim2 that is inducible, and that this upregulated transcript is translated less efficiently compared to the canonical isoform. This novel finding goes against the existing assumption that induced gene expression results in induced protein expression. (Fig. 1I, Fig. 2, Fig. 4). FLAIR-identified transcripts (*33*) show three clear transcriptional start sites (TSS) for *Aim2* and only one of those TSSs is inflammatory inducible (Fig. 2C-D). RT-qPCR further solidifies that the annotated TSS of *Aim2* is not inducible, while the unannotated TSS of *Aim2* is LPS inducible (Fig. 2E-H). This result highlights the need for cell-type specific transcriptome annotations if one is to have a complete understanding of the transcriptome and proteome of a given cell.

We further investigated what drove the expression of this new *Aim2* isoform, as well as what drove the expression of all the AFE genes. Using ATAC-seq (*46*, *50*) and ChIP-seq (*46*) data sets we were able to determine that the AFE events were driven partially by chromatin accessibility and inflammatory specific transcription factors, while 50% were unaccounted for (Fig. 3A). Further analysis incorporating more transcription factors will be necessary to determine the regulatory mechanism. Interestingly, the annotated *Aim2* promoter accessibility is constitutively open across all hematopoietic cells, while the unannotated *Aim2* promoter is only accessible in myeloid progenitors or terminally differentiated cells (SFig. 6A), meaning that the novel

bioRxiv preprint doi: https://doi.org/10.1101/2020.07.06.190330; this version posted July 6, 2020. The copyright holder for this preprint (which was not certified by peer review) is the author/funder. All rights reserved. No reuse allowed without permission.

mechanism of *Aim2* regulation is specific to myeloid cells only. Furthermore, *Aim2* annotated and unannotated promoter usage is not driven by chromatin accessibility (SFig. 6B-C) but is solely driven by the activation of inflammatory specific transcription factors (Fig. 3B-E).

There is no difference in the open reading frame of the novel isoform of Aim2 when compared to the annotated transcript, therefore we turned our attention to a possible regulatory mechanism within the 5′UTR (*79*). Broadly, UTRs play crucial roles in the post-transcriptional regulation of gene expression, including alteration of the mRNA translational efficiency (*80*), subcellular localization (*81*) and stability (*82*). Post-transcriptional regulatory mechanisms of Aim2 have not been previously studied. Using RegRNA2.0 (*53*) we identified an Iron Responsive Element (IRE), a unique regulatory motif within the novel 5′UTR of Aim2 (Fig. 4F). Utilizing a GFP reporter plasmid, we were able to determine that the IRE motif was functional, by recapitulating the same experiments used on the protein Ferritin, the first functional IRE motif ever studied (*83*). Finally, we showed the inflammatory specific mechanism regulating AIM2 protein expression by performing a western blot on primary BMDMs with and without Ferric Ammonium Citrate (FAC) during a 72 hr LPS time-course experiment. AIM2 protein is basally expressed and while the transcript is inducible, specifically the novel isoform we identify here we do not observe an increase in expression of AIM2 protein by western blot. In fact, we find that AIM2 protein decreases following inflammation and this can be reversed by iron supplementation. This could be a critical regulatory step that has evolved to ensure the AIM2 pathway is switched off following its formation and activation of the inflammasome.

These results demonstrate that the inflammatory specific mRNA isoform of *Aim2* has lower translational efficiency than the canonical form and that protein translation can be increased by the addition of iron. Crane *et al.* (*84*) demonstrate that ROS can contribute to activation of AIM2

bioRxiv preprint doi: https://doi.org/10.1101/2020.07.06.190330; this version posted July 6, 2020. The copyright holder for this preprint (which was not certified by peer review) is the author/funder. All rights reserved. No reuse allowed without permission.

inflammasome in mouse macrophages. Our proposed mechanism of translational regulation of AIM2, is through an Iron Responsive Element (IRE), which is known to directly interact with IRP proteins (*55–57*). Interestingly, IRP2 degradation can be driven not only through iron, but also through ROS and RNS (*85*), further supporting this novel IRE regulatory mechanism of AIM2 protein expression. Finally, Cheng *et al.* has shown that AIM2 is regulated by oxidative stress and show that over activation of AIM2 inflammasome can contribute to pancreatic tumorigenesis, all within the environment of mitochondrial iron overload (*86*). This newly identified isoform, with an IRE specific translational mechanism provides mechanistic understanding to these recent studies of Aim2 (*84*, *86*). These findings could have significance for better understanding the mechanisms driving pathology in inflammatory disease such as systemic lupus erythematosus (SLE) (*87*). AIM2 expression levels have been correlated with severity of inflammation in SLE patients (*88*) and it is well known that iron is dysregulated in this disease (*89*). It is possible that AIM2 levels remain high in SLE patients due to dysregulated iron; therefore, homeostasis in macrophages cannot be maintained.

In summary, signaling within macrophages has the ability to fight infection but also contribute to pathological inflammation associated with a wide variety of diseases. While there are multiple regulatory checkpoints in place to control inflammation, we propose that alternative splicing and translational regulation play critical roles in maintaining this type of control. A better understanding of the molecular mechanisms that control inflammatory-regulated genes, including *Aim2,* could provide new targets for therapeutic intervention of autoimmune and inflammatory diseases.

Acknowledgements:

bioRxiv preprint doi: https://doi.org/10.1101/2020.07.06.190330; this version posted July 6, 2020. The copyright holder for this preprint (which was not certified by peer review) is the author/funder. All rights reserved. No reuse allowed without permission.

We thank Eric Martin for sharing his time and knowledge on HOMER. We would also like to thank Alison Tang with sharing her knowledge and assisting with FLAIR isoform analysis. Finally, we would like to thank Kevin S. Johnson and Karen Ottemann who lent reagents for the IRE mutagenesis experiments.

Funding:

This work was partially supported by a Special Research Grant/Collaborative Research Grant from the UCSC Committee on Research (COR) to ANB and SCa. Additional funding support from NIH HG010053 (ANB and MA) and Oxford Nanopore Research Grant SC20130149 (MA).

Author contributions:

EKR performed all the molecular biology experiments from Fig 1, 2 and 4. PJ carried out all the bioinformatic analyses on alternative splicing from both mouse and human LPS stimulated macrophages. SCo assisted in designing of cloning experiments and generating samples for polysome profiling in Fig 4. MC performed promoter and AFE analysis in Fig 3 and EKR performed HOMER promoter analysis on Aim2 promoters. BS cultured the primary mouse macrophages and generated the illumina, while RAS generated the Nanopore RNA-sequencing libraries. RS analyzed the Nanopore sequencing datasets, with assistance from MJ. RS performed the human primary macrophage culturing and sequencing experiences. SMC assisted in the construction of the Iron related experiments and background knowledge in the field. ANB, SCa, EKR and PJ conceived and coordinated the project. EKR, PJ, ANB and SCa wrote the manuscript with input from all other co-authors.

Competing interests:

bioRxiv preprint doi: https://doi.org/10.1101/2020.07.06.190330; this version posted July 6, 2020. The copyright holder for this preprint (which was not certified by peer review) is the author/funder. All rights reserved. No reuse allowed without permission.

MA holds options in Oxford Nanopore Technologies (ONT). MA is a paid consultant to ONT. MA and ANB received reimbursement for travel, accommodation and conference fees to speak at events organized by ONT. MA is an inventor on 11 UC patents licensed to ONT (6,267,872, 6,465,193, 6,746,594, 6,936,433, 7,060,50, 8,500,982, 8,679,747, 9,481,908, 9,797,013, 10,059,988, and 10,081,835). MA received research funding from ONT.

Data and Materials Availability:

All data are available in the manuscript or the supplementary materials. RNA-seq raw data have been deposited in the NCBI Gene Expression Omnibus database under accession numbers GSE141754.

Figure Legends:

Figure 1: Global profiling of the cellular alternative splicing landscape in human and mouse macrophages post-inflammatory. (A) Diagram of RNA-seq library generation. **(B)** Categorization of significant splicing events in human and mouse macrophage. **(C)** Categorization of significant splicing events found in mouse BMDM +/- 6hrs LPS prior to and after incorporating high-confidence long-read isoforms identified using Nanopore sequencing. **(D)** Venn diagram representing unique and common genes with AFE events found in Nanopore or Illumina RNA-seq of primary BMDMs post-inflammatory stimulation. Volcano plots of all differentially expressed genes from RNA-seq of either human **(E)** or mouse **(F)** macrophages. Genes highlighted in red undergo significant AFE changes following inflammation. Schematic of AFE inclusion and exclusion isoforms, followed by RT-PCR gel results and PSI calculation for *Argehf7* **(G)** *Denr* **(H)** and *Aim2* **(I)**, were performed in biological triplicates, p-value assessed using student's t-test.

bioRxiv preprint doi: https://doi.org/10.1101/2020.07.06.190330; this version posted July 6, 2020. The copyright holder for this preprint (which was not certified by peer review) is the author/funder. All rights reserved. No reuse allowed without permission.

Figure 2: Identification of an unannotated promoter in *Aim2*. (A-B) The top track, in black, represents ChIP-seq data for a macrophage-specific transcription factor, PU.1. Peaks represent possible promoter regions; two distinct peaks of equal height are present at the annotated transcriptional start site for *Aim2* and about 1kb upstream of the transcriptional start site (TSS). The middle track, in orange, represents basal transcription in bone marrow-derived macrophages (BMDMs), while the bottom track, in purple, represents active transcription in BMDMs 6 hr LPS post treatment. **(C)** *Aim2* transcript isoforms identified in BMDMs by native RNA long-read sequencing through FLAIR analysis. Transcripts are categorized by promoter, denoted by grey, orange or purple. **(D)** The bar-chart represents data from long-read sequencing showing the abundance of each transcript isoform from BMDMs +/- 6hrs LPS. **(E-H)** qRT-PCR was performed in biological triplicate, on primary BMDM RNA extracts that had been stimulated with LPS for indicated time points.

Figure 3: Novel inflammatory promoter of *Aim2* is regulated by IRF3 and p65. (A) UpSet plot showing the number of AFE events out of 77 total that have differential transcription factor binding and differential chromatin accessibility and all combinations of these sets. **(B)** mm9 genome browser shot between chr1:175,348,283-175,351,422 of ChIP-seq for IRF3 and p65 binding in BMDMs. **(C)** Venn diagram of all motifs defined using HOMER analysis within the annotated and unannotated promoter regions. **(D-E)** DAVID analysis examining the gene ontology of transcription factors at the annotated and unannotated promoters of *Aim2*.

Figure 4: Unannotated 5′UTR of *Aim2* negatively regulates translation through a single iron responsive element. (A) Schematic of annotated and unannotated 5′UTR of most prevalent *Aim2* isoforms in mouse macrophages. **(B)** Diagram of cloning strategy of *Aim2's* 5′UTR in GFP plasmid. **(C)** Transfection strategy of 5′UTR-GFP plasmids co-transfected with an mCherry

bioRxiv preprint doi: https://doi.org/10.1101/2020.07.06.190330; this version posted July 6, 2020. The copyright holder for this preprint (which was not certified by peer review) is the author/funder. All rights reserved. No reuse allowed without permission.

control plasmid at a 1 to 1 ratio in 293T cells. **(D-E)** Flow cytometry of 293T cells 72 hr posttransfection with control annotated and unannotated 5′UTR of *Aim2* to measure GFP and mCherry (Ctl) protein fluorescence. **(F)** Using RegRNA2.0 a single iron-responsive element (IRE) was found in the alternative 5′UTR, in addition to multiple musashi binding elements (MBE). **(G)** Diagram of how an IRE functions in the cytoplasm of a cell within a 5′UTR. With low or normal levels of iron, Iron Binding Proteins (IRP1 or IRP2) bind to IRE elements and block translation. During high levels of iron, within a cell, IRP1 is sequestered by iron-sulfur (Fe-S) clusters and IRP2 is degraded, therefore allowing translation of the protein. **(H-I)** Flow cytometry of 293T cells 72 hr post-transfection of mCherry (Ctl), along with an annotated 5′UTR-GFP plasmid, unannotated 5′UTR-GFP plasmid, or a GFP plasmid containing the unannotated 5′UTR without the defined iron-responsive element (IRE). **(J-K)** Flow cytometry of 293T cells +/- 100uM ferric ammonium citrate (FAC) 72 hr post-transfection of mCherry (Ctl), along with an annotated 5′UTR-GFP plasmid or unannotated 5′UTR-GFP plasmid. **(L)** Overview of the polysome profiling protocol to analyze translation activity. **(M)** Cytoplasmic lysates from control and LPS treated cells were fractionated through sucrose gradients. Global RNA polysome profiles generated by the density gradient fractionation system are shown. A representative plot from stimulated primary BMDM fractionated samples is shown. The experiment was performed 4 times. **(N-P)** The relative distribution of *Gapdh* mRNA, encoding a housekeeping protein, *Neat1* long non-coding RNA (lncRNA) and *Aim2* mRNA were measured by RT-qPCR analysis of RNA using isoform-specific primer sets. Each of the gradient fractions are calculated as relative enrichment when compared to unfractionated input mRNA, standard deviation represents technical triplicate. **(Q)** Protein lysates of time course LPS stimulation of 0hr, 6hr, 24hr, 48hr and 72hr without and with 100uM of Ferric Ammonium Citrate (FAC, iron) added to immortalized WT BMDMs. Western blot performed on

bioRxiv preprint doi: https://doi.org/10.1101/2020.07.06.190330; this version posted July 6, 2020. The copyright holder for this preprint (which was not certified by peer review) is the author/funder. All rights reserved. No reuse allowed without permission.

AIM2 and B-ACTIN. **(R)** Western blot quantification performed in FIJI, standard deviation represents biological triplicates, p-value assessed using student's t-test.

bioRxiv preprint doi: https://doi.org/10.1101/2020.07.06.190330; this version posted July 6, 2020. The copyright holder for this preprint (which was not certified by peer review) is the author/funder. All rights reserved. No reuse allowed without permission.

Materials and Methods

Human PBMC derived macrophage differentiation and in vitro stimulation

Human peripheral blood mononuclear cells (PBMC) were enriched by density gradient centrifugation of peripheral blood from healthy human donors through a Ficoll-Paque PLUS (GE Healthcare) gradient. Monocytes were isolated from PBMC by negative selection using the EasySep™ Human Monocyte Isolation Kit (STEMCELL Technologies) according to the manufacturer's instructions. To differentiate monocytes into macrophages, recombinant human M-CSF (50ng/mL) was used in RPMI-1640 medium with 10% FBS, 2mM L-glutamine, 10mM HEPES, 1mM sodium pyruvate, 100U/ml penicillin, and 100 µg/mL streptomycin. The culture medium which contained fresh recombinant human M-CSF was replaced every 2 days.

Cell culture, Mouse Macrophage Differentiation and Stimulation

Cells were cultured in D-MEM with 10% fetal bovine serum (FCS) supplemented with penicillin/streptomycin or ciprofloxacin. Primary BMDM were generated by cultivating erythrocyte-depleted bone marrow cells in the presence of 30% L929 supernatant and the cells were used for experiments 6-9 days after differentiation. J2Cre virus (Blasi et al., 1989) was used on day 3/4 after isolation of bone marrow cells to establish transformed BMDM cell lines. BMDMs were cultivated in the presence of J2Cre virus for 48h and L929 was then gradually tapered off over 6-10 weeks depending on the growth pattern of transformed cells.

In vitro stimulation of macrophages

Bone derived macrophage cells were primed with 100uM of Ammonium Ferric Citrate (FAC) for 24hrs prior to TLR stimulation. Bone marrow derived macrophage cells were stimulated with Toll-like receptor (TLR) ligands for the indicated time points using the following concentrations:

bioRxiv preprint doi: https://doi.org/10.1101/2020.07.06.190330; this version posted July 6, 2020. The copyright holder for this preprint (which was not certified by peer review) is the author/funder. All rights reserved. No reuse allowed without permission.

428 Lipopolysaccharide (LPS) 100ng/ml (TLR4). For RNA and protein isolation, 1-2x10^6 cells were
429 seeded in 12-well format.

430 Cloning Strategy for 5'UTR GFP Plasmid

431 The GFP reporter plasmid was CMV-Zeo-t2A-GFP. Zeocin is flanked by NheI and AgeI. The
432 sequence of the annotated and unannotated 5'UTR were used as defined by the UCSC RefSeq and
433 our sequencing results to be. Using KAPA HiFi HotStart ReadyMix PCR Kit (Kapa Biosystems)
434 the two 5'UTRs were amplified from cDNA.

5'UTR	cDNA Sequence
Annotated	TTCCTGTCCTGTCTGCCGCCATGCTTCCTTAACTAGCTGCTAGGTTTTTTCCTTGTCGTGATGAAATCCACCCTCATGGACCTGTAAGTAAAATGTAGACTTGCATAGAGTGCTGTAATCTTACGGCCGAGGTTTCTTTTCAGGCTGATCCTGGGACTGTGAG
Unannotated	TATATCTAAAATACCTCTGGTTGAGACCTCACAGCTGGAGGAGAAACTCTGCTGAGGCTTGTAAAAAGGAAACTGAAAACTAGCATTTGCTTGGGCAGAGCCTTAATATATAATTATTTTGCCCCAGCATCAGGGTTTAGGACTCAGCTATAGGGCCAGGACTAGCCAAGCTTCAAAGTGAAAGAAGATAGTTGAGAGTACTTTCTGCTTTCTGTCTCCCAAGACCTGATTTTCATGATTTTCATGTCCTACTACTCATAGTGAAAATCTTTGTGAGGCGGATGGTTTGAACTCTCAGGACATACACCAGTCCCTGAGTTGAGAACTAAGGCTGCTTTGGAGAGAAGAAAATCCCCTGAGGTAAGTAGACTTGCATAGAGTGCTGTAATCTTACGGCCGAGGTTTCTTTTCAGGCTGATCCT

bioRxiv preprint doi: https://doi.org/10.1101/2020.07.06.190330; this version posted July 6, 2020. The copyright holder for this preprint (which was not certified by peer review) is the author/funder. All rights reserved. No reuse allowed without permission.

	GGGACTGTGAG

Primers:

cDNA_F_Annotated: TTCCTGTCCTGTCTGCCG

cDNA_F_Unannotated: TATATCTAAAATACCTCTGGTTGAGACCTC

cDNA_R_5'UTR: CTCACAGTCCCAGGATCAGC

The 5'UTRs were then PCR amplified with primers containing restriction enzyme sites for AgeI and NheI.

NheI_F_Annotated: GGT**GCTAGC**TTCCTGTCCTGTCTGCC

NheI_F_Unannotated: GGTGGT**GCTAGC**TATATCTAAAATACCTCTGGTTGAGA

AgeI_R_5'UTR: GGT**ACCGGT**CTCACAGTCCCAGGATCAGC

PCR products, as well as the GFP plasmid, were then processed using AgeI and NheI restriction enzymes overnight. These samples were run on a 1% agarose gel. A gel extraction was completed for each band using the PCR clean-up Gel extraction kit (Machery-nagel). The PCR product was confirmed using Sanger Sequencing.

<u>Site Directed Mutagenesis</u>

Set up PCR reaction with 1ul 279 Plasmid, with unannotated Aim2 5'UTR, 5ul 10x Phu buffer, 1ul F primer (0.1ug/ul) [Remove_IRE_F - CCCTGATGCTGGGGCAAAATAATTATAAATGCTAGTTTTCAGTTTC], 1ul R primer (0.1ug/ul) [Remove_IRE_R - GAAACTGAAAACTAGCATTTATAATTATTTTGCCCCAGCATCAGGG], 1ul dNTP (10nM), 1ul Phu polymerase and 40ul dH2O. PCR program: 95°C 1min, 18 cycles of 95°C 30sec, 55°C 1min, 72°C 1min, then end PCR with 72°C 1min and 4°C hold. Add 0.5ul of Dpn1 (NEB)

bioRxiv preprint doi: https://doi.org/10.1101/2020.07.06.190330; this version posted July 6, 2020. The copyright holder for this preprint (which was not certified by peer review) is the author/funder. All rights reserved. No reuse allowed without permission.

to 25ul PCR reaction. Incubate at 37 degrees celsius for 1hr to digest parental DNA. Transform digested and undigested plasmid into DH5α competent cells. Pick ~10-15 colonies and start overnight cultures. Colony PCR plasmids using Dpn1_Colony_PCR_F - TTGGCTAGTCCTGGCCCTAT and Dpn1_Colony_PCR_R - GCTGGTTTAGTGAACCGTCAG to check for 20bp deletion on a 3% Agarose Gel. Grow up colonies that have deletion, miniprep plasmids and send to sequetech for sequence verification.

Transfection of 5'UTR GFP and mCherry Plasmid

A 1:1 ratio of the GFP vector containing the mature sequence of Aim2 5'UTR (annotated or unannotated) or zeocin and a plasmid containing mCherry were transfected into 293T cells for 48-72hrs. A 6-well plate of HEK293Ts were plated the night before with a concentration of $2x10^5$. HEK293Ts cells were primed with 100uM of Ammonium Ferric Citrate (FAC) for 24hrs prior to transfection. Transfection was performed on HEK293Ts (+/- 100uM FAC) using lipofectamine 2000, serum free OPTI-MEM media was used as a transfection reagent according to manufacturer's instructions, and a (1:1) concentration of the 5'UTR GFP reporter plasmid and the mCherry control plasmid. HEK293Ts were visualized via flow cytometry 48-72hrs post transfection.

Maintenance of mice

UCSC and the Institutional Animal Care and Use Committee maintained mice under specific pathogen-free conditions in the animal facilities of `University of California Santa Cruz (UCSC) in accordance with the guidelines.

Polyribosome Profiling

Prior to lysis, cells were treated with cycloheximide (100 mg/mL), 10 min at 37°C 5%CO2. Cells were washed three times with ice cold PBS and lysed in ice cold buffer A (0.5% NP40, 20 mM

bioRxiv preprint doi: https://doi.org/10.1101/2020.07.06.190330; this version posted July 6, 2020. The copyright holder for this preprint (which was not certified by peer review) is the author/funder. All rights reserved. No reuse allowed without permission.

Tris HCl pH 7.5, 100 mM KCl and 10 mM MgCl2). Lysates were passed three times through a 23G needle and incubated on ice for 7 min. Extracts were then centrifuged at 10K rpm for 7 min at 4°C. The supernatant was collected as crude cytosolic extract. Cytosolic extracts were overlaid on 10%–50% sucrose gradients prepared in 20 mM Tris HCl pH 7.5, 100 mM KCl and 10 mM MgCl2 buffer (prepared using the Gradient Station, Biocomp Instruments). Gradients were then ultracentrifuged at 40K rpm for 1h 20 min at 4°C using an SW41 in a Beckman ultracentrifuge. Individual polyribosome fractions were subsequently purified using a Gradient Station (Biocomp Instruments) and stored in (1:3) TRI Reagent.

<u>RNA isolation, RT-qPCR</u>

Total cellular RNA from BMDM cell lines or tissues was isolated using the Direct-zol™ RNA MiniPrep Kit (Zymo Research) according to manufacturer's instructions. RNA was quantified and controlled for purity with a nanodrop spectrometer. (Thermo Fisher). For RT-qPCR, 500-1000 ng were reversely transcribed (iScript Reverse Transcription Supermix, Biorad) followed by RT-PCR (iQ SYBRgreen Supermix, Biorad) using the cycling conditions as follows: 50°C for 2 min, 95°C for 2 min followed by 40 cycles of 95°C for 15 sec, 60°C for 30 sec and 72°C for 45 sec. The melting curve was graphically analyzed to control for nonspecific amplification reactions. Quantitative RT-PCR analysis was performed with the following primers listed below:

Mse_Aim2_F_Annotated: CCGCCATGCTTCCTTAACTA

Mse_Aim2_F_Unannotated: AGGCGGATGGTTTGAACTCT

Mse_Aim2_R_Exon2: TTGAAGCAACTTCCATCTGC

Mse_Aim2_CDS_F: AGTACCGGGAAATGCTGTTG

Mse_Aim2_CDS_R: GAGTGTGCTCCTGGCAATCT

Mse_Gapdh_F: CCAATGTGTCCGTCGTGGATC

bioRxiv preprint doi: https://doi.org/10.1101/2020.07.06.190330; this version posted July 6, 2020. The copyright holder for this preprint (which was not certified by peer review) is the author/funder. All rights reserved. No reuse allowed without permission.

Mse_Gapdh_R: GTTGAAGTCGCAGGAGACAAC

Mse_Neat1_F: TTGGGACAGTGGACGTGTGG

Mse_Neat1_R: TCAAGTGCCAGCAGACAGCA

RT-PCR Validation

RT-PCR validation was completed using three biological replicates. KAPA HiFi HotStart ReadyMix PCR Kit (Kapa Biosystems) and the manufacturer's suggested cycling protocol was used to complete the PCR reaction with the following primers:

Mse_Denr_F1: ATCGCGATAAAGGCTCATTG

Mse_Denr_F2: GCTACCTGTCCTTTTCCCCA

Mse_Denr_R: AACTTGGCACTGTTCTTCGT

Mse_Arhgef7_F1: TGTTGTTCTGGGGTTTGTGA

Mse_Arhgef7_F2: CTGTGTGTTGCAGGTCTACC

Mse_Arhgef7_R: GTGTCACCAAGGAGCTGAGG

Mse_Ncoa7_F1: GTGGTGGAGAAGGAAGAGCT

Mse_Ncoa7_F2: TTCTATTGTGCCAGGCCTGA

Mse_Ncoa7_R: GCATGTTTTCCAGGAGTGCA

Mse_Ampd3_F1: CCCTACTGTAGATGAATCCCCTTA

Mse_Ampd3_F2: GCTGAGCTTTGTGTCTGTGT

Mse_Ampd3_R: GGGGACAGTAAACAGGGACA

Mse_Rcan1_F1: ACTGGAGCTTCATCGACTGC

Mse_Rcan1_F2: GACTGAGAGAGCGAGTCGTT

Mse_Rcan1_R: CATCGGCTGCAGATAAGGGG

Hu_NCOA7_F1: TGTTCAGTGGTCTCCCGATGTCTATGG

bioRxiv preprint doi: https://doi.org/10.1101/2020.07.06.190330; this version posted July 6, 2020. The copyright holder for this preprint (which was not certified by peer review) is the author/funder. All rights reserved. No reuse allowed without permission.

Hu_NCOA7_R: GGGCCGTAGGACAGGCAGCA

Hu_NCOA7_R2: AGCGTGGCTACAAGTAACTGTGGTGT

Hu_AMPD3_F1: TATGCAAAACAGAGACCTCC

Hu_AMPD3_R: CACTTCAGAGATGTTCAGCT

Hu_AMPD3_F2: CCTGCTTGGTTTTAGAGGAT

Hu_RCAN1_F1: GACTGGAGCTTCATTGACTG

Hu_RCAN1_R: ATTCTGACTCGTTTGAAGCT

Hu_RCAN1_F2: TAGCGCTTTCACTGTAAGAA

Band intensities were measured for each band in each condition and sample using FIJI [Schindelin, J]. The relative abundance of each isoform was calculated using the equation to calculate PSI (PSI = inclusion/ (inclusion + exclusion)) in each condition and sample to validate the computationally derived delta PSI values. A gel extraction was completed for each band using the PCR clean-up Gel extraction kit (Machery-nagel). The PCR product was confirmed using Sanger Sequencing.

Protein Lysate and Western Blot

Cell lysates were prepared in RIPA buffer (50 mM Tris-HCl pH 8.0, 150 mM NaCl, 1 mM EDTA, 1% (v/v) Nonidet P-40, 0.5% (w/v) sodium deoxyxholate, 0.1% (w/v) SDS) containing protease inhibitor cocktail (Roche) and quantified by the Bicinchoninic Acid Assay (BCA) assay (Thermo Fisher). Equivalent masses (15ug) of each sample were resolved by SDS-PAGE and transferred to a polyvinylidene difluoride (PVDF) membrane and Western blotted with either Aim2 (1:1,000; Cell Signaling #63660) and horseradish peroxidase-conjugated b-actin monoclonal antibody (1:5,000, Santa Cruz Biotechnology) were used as a loading control. HRP-conjugated goat anti-rabbit (1:1,500, Biorad) secondary antibodies were used. Image J (*90*) was used for quantification of Western blots.

bioRxiv preprint doi: https://doi.org/10.1101/2020.07.06.190330; this version posted July 6, 2020. The copyright holder for this preprint (which was not certified by peer review) is the author/funder. All rights reserved. No reuse allowed without permission.

549 Alternative splicing quantification

550 After the identification of each alternative splicing event, JuncBASE counts reads supporting the
551 inclusion and exclusion isoform of each event. Isoform abundances are then calculated by dividing
552 the read counts for the isoform by the length of the isoform. Ψ-values for each splicing event are
553 derived from the isoform abundances:

554 PSI Formula:

555 PSI = Inclusion Isoform Abundance / (Inclusion Isoform Abundance + Exclusion Isoform
556 Abundance)

557 Statistical Analysis

558 Error bars represent the standard deviation of biological triplicates. Student's t-tests were
559 performed using GraphPad Prism. Asterisks indicate statistically significant differences between
560 mouse lines (*p> 0.05, **p> 0.01, ***p>0.005).

561 Illumina RNA Sequencing (Human)

562 RNA-seq libraries were prepared with the Illumina TruSeq RNA Sample Preparation kit (Illumina)
563 according to the manufacturer's protocol. Libraries were validated on an Agilent Bioanalyzer
564 2100. Indexed libraries were equimolarly pooled and sequenced on a SE50 (single-end 50 base
565 pair) Illumina HiSeq2500 lane, which yielded an average of about 30×10^6 reads/sample.

566 Illumina RNA Sequencing (Mouse)

567 For generation of RNASequencing libraries, RNA was isolated as described above and the RNA
568 integrity was tested with a BioAnalyzer (Agilent Technologies) or FragmentAnalyzer (Advanced
569 Analytical). For RNASequencing target RIN score of input RNA (500-1000ng) usually had a
570 minimum RIN score of 8. RNASequencing libraries were prepared with TruSeq stranded RNA
571 sample preparation kits (Illumina), depletion of ribosomal RNA was performed by positive

bioRxiv preprint doi: https://doi.org/10.1101/2020.07.06.190330; this version posted July 6, 2020. The copyright holder for this preprint (which was not certified by peer review) is the author/funder. All rights reserved. No reuse allowed without permission.

572 selection of polyA+ RNA. Sequencing was performed on Illumina HighSeq or NextSeq machines.
573 RNA-seq 50bp reads were aligned to the mouse genome (assembly GRCm38/mm10) using
574 TopHat (*91*). The Gencode M13 gtf was used as the input annotation. Differential gene expression
575 specific analyses were conducted with the DESeq (*92*) R package. Specifically, DESeq was used
576 to normalize gene counts, calculate fold change in gene expression, estimate p-values and adjusted
577 p-values for change in gene expression values, and to perform a variance stabilizing transformation
578 on read counts to make them amenable to plotting. Data was submitted to GEO GSE141754.

579 Nanopore Direct RNA Sequencing

580 *Total RNA extraction:* Total RNA was extracted according to Workman *et al.* (*93*). 5 x 10^7 frozen
581 macrophages were resuspended in three ml of TRI-Reagent (Invitrogen AM9738) and vortexed
582 for 5 min. The mixture was incubated at RT for 5 minutes, transferred to 1.5 mL tubes and spun
583 down to remove debris. Supernatant was transferred to fresh tubes and chloroform extracted. The
584 aqueous portion was mixed with an equal volume of isopropanol, incubated for 15 min at RT and
585 centrifuged at 12,000 g at 4C. Pellet was washed twice with 75% ethanol, air dried and
586 resuspended in nuclease free water.

587 *Poly(A) RNA isolation*: One hundred µg aliquots of total RNA preparation were brought to 100 µl
588 in nuclease free water and poly-A selected using NEXTflex Poly(A) Beads (BIOO Scientific
589 Cat#NOVA-512980) according to the manufacturer's instructions. The resulting poly-A RNA
590 solution was stored at -80ºC.

591 *Library preparation and MinION run*: A native RNA sequencing sequencing library was prepared
592 following the ONT SQK-RNA001 using Superscript IV (Thermo Fisher) for the reverse
593 transcriptase step. Sequencing was performed using ONT R9.4 flow cells and the standard
594 MinKNOW protocol.

bioRxiv preprint doi: https://doi.org/10.1101/2020.07.06.190330; this version posted July 6, 2020. The copyright holder for this preprint (which was not certified by peer review) is the author/funder. All rights reserved. No reuse allowed without permission.

Basecalling and sequence alignments: ONT albacore version 2.1.0 was used to baseball Nanopore direct RNA raw signal. We used minimap2 (*94*) with default parameters to align reads to the mm10 mouse genome reference. Following alignment, we used SAMtools (*95*) to filter-out reads with mapping quality (MAPQ) less than 30.

Alignment of Paired-end Mouse RNA-seq data

Bowtie2-build v2.3.1 (*96*) was used to build the index files from GRCm38.p6 mouse (mm10 assembly) genome sequence obtained from Gencode. The index files were then used for completing paired-end alignment of each sample using TopHat2 v2.1.1 (*97*) with parameters: *--segment-length 20, --library-typ fr-firststrand, --no-coverage-search*.

Identification of Splicing Events and Calculating PSI

Human monocyte-derived macrophage +/- LPS and Mouse bone marrow-derived macrophage +/- LPS were each run through JuncBASE v1.2 (*98*) to calculate percent spliced in (PSI) values and identify splicing events. The JuncBASE parameters used for the identification of splicing events and calculation of PSI in Human monocyte derived macrophage +/- LPS are: *-c 1.0 -j [introns from Gencode v24 (hg19 assembly)* (*99*) *--jcn_seq_len 88*. The JuncBASE parameters used for the identification of splicing events and calculation of PSI in Mouse bone marrow-derived macrophage +/- LPS are: *-c 1.0 -j [introns from Gencode M18 (mm10 assembly)*(*99*) *--jcn_seq_len 88*.

Identification of High-Confidence Isoforms from Nanopore Data

FLAIR (full length alternative isoform analysis of RNA) (*100*) was used to assemble the high-confidence isoforms from native RNA sequencing of Mouse BMDM +/- 6hr LPS. FLAIR modules align, correct, and collapse were used for the assembly. Corresponding short read data was used when running the correct module in order to help increase splice-site accuracy. Putative promoter

bioRxiv preprint doi: https://doi.org/10.1101/2020.07.06.190330; this version posted July 6, 2020. The copyright holder for this preprint (which was not certified by peer review) is the author/funder. All rights reserved. No reuse allowed without permission.

regions were obtained using ATAC-seq data from Smale *et al.* and Atianand *et al.* (*101*, *102*) converted to mm10 coordinates using liftOver (*103*), and used when running the collapse module.

Differential Splicing Analysis

Differential splicing analysis was completed using DRIMSeq v1.10.1 (*104*) and the compareSampleSets.py script within JuncBASE. CompareSampleSets.py applies the statistical t-test and DRIMSeq applies the framework of the Dirichlet-multinomial distribution for differential analysis. Each tool was used to apply the respective statistical method in order to determine significant differentially spliced events between control (-LPS) and LPS (+LPS) conditions. The AS_exclusion_inclusion_counts_lenNorm.txt JuncBASE output table from the identification and quantification analysis of each experiment was used as the input table for both compareSampleSets.py and DRIMSeq.

For all experiments, compareSampleSets.py was run using parameters: *--mt_correction BH --which_test t-test --thresh 10 --delta_thresh 5.0*. The following parameters were used for the differential splicing analysis of data from Human monocyte-derived macrophage +/- LPS with DRIMSeq: *min_samps_gene_expr = 8, min_samps_feature_expr = 4, min_gene_expr = 10, min_feature_expr = 0*. The following parameters were used for the differential splicing analysis of data from Mouse bone marrow-derived macrophage +/- LPS with DRIMSeq: *min_samps_gene_expr = 6, min_samps_feature_expr = 3, min_gene_expr = 10, min_feature_expr = 0*. Following differential splicing analysis using each tool, genes with significant differential splicing events were filtered for using thresholds of a corrected/adjusted p-value ≤ 0.25 and a $|\Delta \text{ PSI}| \geq 10$. Within each category of event type, the union of genes with significant events identified using compareSampleSets.py and DRIMSeq within each experiment

bioRxiv preprint doi: https://doi.org/10.1101/2020.07.06.190330; this version posted July 6, 2020. The copyright holder for this preprint (which was not certified by peer review) is the author/funder. All rights reserved. No reuse allowed without permission.

640 was used for further comparison. Novel intron retention events, annotated with a "N," were
641 removed for further analyses.

642 Creating merged reference annotation files and incorporating nanopore

643 The *isoforms.gtf* output file from FLAIR collapse was combined with the Gencode M18 (mm10
644 assembly) basic annotation using cuffmerge from Cufflinks v2.2.1 (*105*) with parameter: -s
645 GRCm38.p6.genome.fa. Similarly, the *isoforms.gtf* output file was combined with the Gencode
646 M18 (mm10 assembly) comprehensive annotation with parameter: -s GRCm38.p6.genome.fa.
647 The resulting comprehensive annotation output file was used to generate an intron coordinate file
648 for the identification of splicing events and calculating PSI of splicing events found in Mouse
649 Bone-marrow derived macrophage +/- 6hr LPS using JuncBASE with parameters: *-c 1.0, -j [intron*
650 *coordinates from merged comprehensive annotation], --jcn_seq_len 238*. Parameters used for
651 finding significantly differentially spliced events using compareSampleSets.py from JuncBASE
652 are: *--mt_correction BH --which_test t-test --thresh 10 --delta_thresh 5.0*. Parameters used for
653 finding significantly differentially spliced events using DRIMSeq are: *min_samps_gene_expr =*
654 *6, min_samps_feature_expr = 3, min_gene_expr = 10, min_feature_expr = 0*.

655 Gene Expression Analysis

656 DESeq2 v1.22.2 (*106*) was used to create counts tables and complete differential gene expression
657 analysis on RNA-seq data from Human monocyte-derived macrophage +/- 18hr LPS and Mouse
658 BMDM +/- 6hr LPS experiments. The sample conditions used were "control" and "LPS." Data
659 was plotted using ggplot2 v3.1.1 (*107*). Significance thresholds were set to $|\log2FC| \geq 2$ and
660 adjusted p-value ≤ 0.05. The list of genes with significant AFE events were then highlighted on
661 the appropriate graphs.

662 Creating and comparing gene lists

bioRxiv preprint doi: https://doi.org/10.1101/2020.07.06.190330; this version posted July 6, 2020. The copyright holder for this preprint (which was not certified by peer review) is the author/funder. All rights reserved. No reuse allowed without permission.

For each experiment, a table with the union of significant events found using DRIMSeq and compareSampleSets.py was created. A list of genes with significant events was generated for each experiment using this table. BioVenn (*108*) and DrawVenn (*94*) were then used to remove duplicate gene names and compare the lists of genes to find unique and common genes between experiments.

Differential chromatin accessibility

Raw ATAC-seq fastq sequence files were published in Tong *et al.* (*102*) and pulled from the GEO accession number GSE67357. A bowtie2 (*96*) index file was created from the GENCODE mm10 version M18 genome annotation file and the untreated and LPS treated ATAC-seq reads were aligned using the created index file with the default bowtie2 parameters. Peaks were then called separately by treatment type on untreated and treated samples using the ENCODE published ATAC-seq peak calling pipeline (https://github.com/ENCODE-DCC/atac-seq-pipeline) using the aligned reads as sequence input. Parameters that were used followed the basic JSON input file template, using an IDR threshold of 0.05. Peaks from both conditions were then merged using bedtools merge (*109*) if the tail ends were less than 10bp away from each other, in order to create a set of consensus peaks from both conditions. A GFF file was created from the merged peaks, assigning a unique ID to each peak. This GFF file was provided to HTSeq-count (*110*) along with the aligned reads for each condition in each replicate to count reads aligning to the unique peaks. The read count matrix was provided to DESeq2 (*106*) to call differential peaks. All peaks were considered significant if log2FC $\geq$ 0.8 and p-value $\leq$ 0.15.

Differential transcription factor binding

ChIP-seq fastq sequencing files for the NF-κB subunit p65 and interferon transcription factor Irf3 were downloaded from the GEO accession number GSE67357 published by Tong *et al.* (*102*).

bioRxiv preprint doi: https://doi.org/10.1101/2020.07.06.190330; this version posted July 6, 2020. The copyright holder for this preprint (which was not certified by peer review) is the author/funder. All rights reserved. No reuse allowed without permission.

ChIP-seq samples for input control, untreated, and LPS treatment were aligned using bowtie2 (*96*) to the mm10 version M18 mouse genome annotation with default parameters. Peaks were separately called between untreated and treated conditions using the ENCODE published ChIP-seq peak calling pipeline (https://github.com/ENCODE-DCC/chip-seq-pipeline2) from the aligned reads. The aligned input control reads were input as genomic background to account for noise in ChIP-seq experiments. The basic JSON input template file was used, using an IDR threshold of 0.05. Differential peak analysis was done using the HOMER suite designed for ChIP-seq data (*111*). Consensus peaks from both conditions were merged using mergePeaks within HOMER, reporting the direct overlap between peaks. Tag directories were created to count reads for each aligned sequence file with TagDirectory. The merged consensus peaks were then annotated for raw read counts using the tag directories for each replicate and condition with the annotatePeaks.pl tool. Annotated consensus peaks were provided to getDiffExpression.pl, normalizing to total read counts. Peaks were considered significant if they had a p-value ≤ 0.25 and log2FC ≥ 1.

<u>AFE event overlap</u>

To identify differential transcription factor binding and chromatin remodeling at the promoters of the observed alternative first exon events, the coordinates of the alternate first exon were determined from the statistical testing results. Significant (p-value ≤ 0.05) alternative first exon events were first filtered out from all results. For all significant results, if the inclusion exon had a Δ PSI ≥ 10, the inclusion exon coordinates from the JuncBASE table were used as the coordinates for that splicing event. If the inclusion exon had a Δ PSI ≤ -10, all other inclusion exons for that splicing event from the statistical testing (DRIMSeq or t-test) were considered, and any inclusion exon with Δ PSI > 10 was used. Redundant events with the same exon coordinates were then

bioRxiv preprint doi: https://doi.org/10.1101/2020.07.06.190330; this version posted July 6, 2020. The copyright holder for this preprint (which was not certified by peer review) is the author/funder. All rights reserved. No reuse allowed without permission.

filtered out, leading to a final set of 77 exon coordinates. The coordinates were then extended to include 10kbp upstream of the exon. Overlap of differential chromatin accessibility and different transcription factor binding was done using bedtools intersect (*109*) with the significant differential peak coordinates and the alternative first exon 10kbp upstream region, returning the coordinates of the exon that show differential chromatin accessibility or transcription factor binding.

bioRxiv preprint doi: https://doi.org/10.1101/2020.07.06.190330; this version posted July 6, 2020. The copyright holder for this preprint (which was not certified by peer review) is the author/funder. All rights reserved. No reuse allowed without permission.

References

1. R. Medzhitov, C. A. Janeway, Innate immune recognition and control of adaptive immune responses. *Semin. Immunol.* **10**, 351–353 (1998).

2. A. A. Pai, G. Baharian, A. Pagé Sabourin, J. F. Brinkworth, Y. Nédélec, J. W. Foley, J.-C. Grenier, K. J. Siddle, A. Dumaine, V. Yotova, Z. P. Johnson, R. E. Lanford, C. B. Burge, L. B. Barreiro, Widespread Shortening of 3' Untranslated Regions and Increased Exon Inclusion Are Evolutionarily Conserved Features of Innate Immune Responses to Infection. *PLoS Genet.* **12**, e1006338 (2016).

3. K. Hamidzadeh, S. M. Christensen, E. Dalby, P. Chandrasekaran, D. M. Mosser, Macrophages and the Recovery from Acute and Chronic Inflammation. *Annu. Rev. Physiol.* **79**, 567–592 (2017).

4. Y. Zhou, Y. Hong, H. Huang, Triptolide Attenuates Inflammatory Response in Membranous Glomerulo-Nephritis Rat via Downregulation of NF-κB Signaling Pathway. *Kidney Blood Press. Res.* **41**, 901–910 (2016).

5. S. Boudreault, C. Martenon-Brodeur, M. Caron, J.-M. Garant, M.-P. Tremblay, V. E. S. Armero, M. Durand, E. Lapointe, P. Thibault, M. Tremblay-Létourneau, J.-P. Perreault, M. S. Scott, G. Lemay, M. Bisaillon, Global Profiling of the Cellular Alternative RNA Splicing Landscape during Virus-Host Interactions. *PLoS ONE*. **11**, e0161914 (2016).

6. P. Ivanov, P. Anderson, Post-transcriptional regulatory networks in immunity. *Immunol. Rev.* **253**, 253–272 (2013).

7. Y. Wang, J. Liu, B. O. Huang, Y.-M. Xu, J. Li, L.-F. Huang, J. Lin, J. Zhang, Q.-H. Min, W.-M. Yang, X.-Z. Wang, Mechanism of alternative splicing and its regulation. *Biomed Rep*. **3**, 152–158 (2015).

8. A. Ergun, G. Doran, J. C. Costello, H. H. Paik, J. J. Collins, D. Mathis, C. Benoist, ImmGen Consortium, Differential splicing across immune system lineages. *Proc. Natl. Acad. Sci. U.S.A.* **110**, 14324–14329 (2013).

9. C. A. Wells, A. M. Chalk, A. Forrest, D. Taylor, N. Waddell, K. Schroder, S. R. Himes, G. Faulkner, S. Lo, T. Kasukawa, H. Kawaji, C. Kai, J. Kawai, S. Katayama, P. Carninci, Y. Hayashizaki, D. A. Hume, S. M. Grimmond, Alternate transcription of the Toll-like receptor signaling cascade. *Genome Biol.* **7**, R10 (2006).

bioRxiv preprint doi: https://doi.org/10.1101/2020.07.06.190330; this version posted July 6, 2020. The copyright holder for this preprint (which was not certified by peer review) is the author/funder. All rights reserved. No reuse allowed without permission.

10. M. Beyer, M. R. Mallmann, J. Xue, A. Staratschek-Jox, D. Vorholt, W. Krebs, D. Sommer, J. Sander, C. Mertens, A. Nino-Castro, S. V. Schmidt, J. L. Schultze, High-resolution transcriptome of human macrophages. *PLoS ONE*. **7**, e45466 (2012).

11. D. M. Bhatt, A. Pandya-Jones, A.-J. Tong, I. Barozzi, M. M. Lissner, G. Natoli, D. L. Black, S. T. Smale, Transcript dynamics of proinflammatory genes revealed by sequence analysis of subcellular RNA fractions. *Cell*. **150**, 279–290 (2012).

12. R. G. de Bruin, L. Shiue, J. Prins, H. C. de Boer, A. Singh, W. S. Fagg, J. M. van Gils, J. M. G. J. Duijs, S. Katzman, A. O. Kraaijeveld, S. Böhringer, W. Y. Leung, S. M. Kielbasa, J. P. Donahue, P. H. J. van der Zande, R. Sijbom, C. M. A. van Alem, I. Bot, C. van Kooten, J. W. Jukema, H. Van Esch, T. J. Rabelink, H. Kazan, E. A. L. Biessen, M. Ares, A. J. van Zonneveld, E. P. van der Veer, Quaking promotes monocyte differentiation into pro-atherogenic macrophages by controlling pre-mRNA splicing and gene expression. *Nat Commun*. **7**, 10846 (2016).

13. N. Haque, R. Ouda, C. Chen, K. Ozato, J. R. Hogg, ZFR coordinates crosstalk between RNA decay and transcription in innate immunity. *Nat Commun*. **9**, 1145 (2018).

14. W. J. Janssen, T. Danhorn, C. Harris, K. J. Mould, F. F.-Y. Lee, B. R. Hedin, A. D'Alessandro, S. M. Leach, S. Alper, Inflammation-Induced Alternative Pre-mRNA Splicing in Mouse Alveolar Macrophages. *G3 (Bethesda)*. **10**, 555–567 (2020).

15. J. Lin, Y. Hu, S. Nunez, A. S. Foulkes, B. Cieply, C. Xue, M. Gerelus, W. Li, H. Zhang, D. J. Rader, K. Musunuru, M. Li, M. P. Reilly, Transcriptome-Wide Analysis Reveals Modulation of Human Macrophage Inflammatory Phenotype Through Alternative Splicing. *Arterioscler. Thromb. Vasc. Biol.* **36**, 1434–1447 (2016).

16. H. Liu, P. A. Lorenzini, F. Zhang, S. Xu, M. S. M. Wong, J. Zheng, X. Roca, Alternative splicing analysis in human monocytes and macrophages reveals MBNL1 as major regulator. *Nucleic Acids Res.* **46**, 6069–6086 (2018).

17. B. P. O'Connor, T. Danhorn, L. De Arras, B. R. Flatley, R. A. Marcus, E. Farias-Hesson, S. M. Leach, S. Alper, Regulation of toll-like receptor signaling by the SF3a mRNA splicing complex. *PLoS Genet.* **11**, e1004932 (2015).

18. A. Pandya-Jones, D. M. Bhatt, C.-H. Lin, A.-J. Tong, S. T. Smale, D. L. Black, Splicing kinetics and transcript release from the chromatin compartment limit the rate of Lipid A-induced gene expression. *RNA*. **19**, 811–827 (2013).

19. K. W. Lynch, Consequences of regulated pre-mRNA splicing in the immune system. *Nat. Rev. Immunol.* **4**, 931–940 (2004).

bioRxiv preprint doi: https://doi.org/10.1101/2020.07.06.190330; this version posted July 6, 2020. The copyright holder for this preprint (which was not certified by peer review) is the author/funder. All rights reserved. No reuse allowed without permission.

20. A. Schaub, E. Glasmacher, Splicing in immune cells-mechanistic insights and emerging topics. *Int. Immunol.* **29**, 173–181 (2017).

21. R. Z. Blumhagen, B. R. Hedin, K. C. Malcolm, E. L. Burnham, M. Moss, E. Abraham, T. J. Huie, J. A. Nick, T. E. Fingerlin, S. Alper, Alternative pre-mRNA splicing of Toll-like receptor signaling components in peripheral blood mononuclear cells from patients with ARDS. *Am. J. Physiol. Lung Cell Mol. Physiol.* **313**, L930–L939 (2017).

22. F. Shakola, P. Suri, M. Ruggiu, Splicing Regulation of Pro-Inflammatory Cytokines and Chemokines: At the Interface of the Neuroendocrine and Immune Systems. *Biomolecules*. **5**, 2073–2100 (2015).

23. W. Deng, M. Shi, M. Han, J. Zhong, Z. Li, W. Li, Y. Hu, L. Yan, J. Wang, Y. He, H. Tang, V. Deubel, X. Luo, Q. Ning, B. Sun, Negative regulation of virus-triggered IFN-beta signaling pathway by alternative splicing of TBK1. *J. Biol. Chem.* **283**, 35590–35597 (2008).

24. L. De Arras, S. Alper, Limiting of the innate immune response by SF3A-dependent control of MyD88 alternative mRNA splicing. *PLoS Genet.* **9**, e1003855 (2013).

25. K.-J. Han, Y. Yang, L.-G. Xu, H.-B. Shu, Analysis of a TIR-less splice variant of TRIF reveals an unexpected mechanism of TLR3-mediated signaling. *J. Biol. Chem.* **285**, 12543–12550 (2010).

26. S. Carpenter, E. P. Ricci, B. C. Mercier, M. J. Moore, K. A. Fitzgerald, Post-transcriptional regulation of gene expression in innate immunity. *Nat. Rev. Immunol.* **14**, 361–376 (2014).

27. S. Ghiasvand, B. Bakhshinejad, S. J. Mowla, M. Sadeghizadeh, Potential roles of 5′ UTR and 3′ UTR regions in post-trans-criptional regulation of mouse Oct4 gene in BMSC and P19 cells. *Iran J Basic Med Sci*. **17**, 490–496 (2014).

28. K. Leppek, R. Das, M. Barna, Functional 5’ UTR mRNA structures in eukaryotic translation regulation and how to find them. *Nat. Rev. Mol. Cell Biol.* **19**, 158–174 (2018).

29. M. Kramer, C. Sponholz, M. Slaba, B. Wissuwa, R. A. Claus, U. Menzel, K. Huse, M. Platzer, M. Bauer, Alternative 5’ untranslated regions are involved in expression regulation of human heme oxygenase-1. *PLoS ONE*. **8**, e77224 (2013).

30. A. M. Resch, A. Y. Ogurtsov, I. B. Rogozin, S. A. Shabalina, E. V. Koonin, Evolution of alternative and constitutive regions of mammalian 5’UTRs. *BMC Genomics*. **10**, 162 (2009).

bioRxiv preprint doi: https://doi.org/10.1101/2020.07.06.190330; this version posted July 6, 2020. The copyright holder for this preprint (which was not certified by peer review) is the author/funder. All rights reserved. No reuse allowed without permission.

31. E. Mariella, F. Marotta, E. Grassi, S. Gilotto, P. Provero, The Length of the Expressed 3' UTR Is an Intermediate Molecular Phenotype Linking Genetic Variants to Complex Diseases. *Front Genet*. **10**, 714 (2019).

32. C. Mayr, Evolution and Biological Roles of Alternative 3'UTRs. *Trends Cell Biol.* **26**, 227–237 (2016).

33. R. E. Workman, A. D. Tang, P. S. Tang, M. Jain, J. R. Tyson, R. Razaghi, P. C. Zuzarte, T. Gilpatrick, A. Payne, J. Quick, N. Sadowski, N. Holmes, J. G. de Jesus, K. L. Jones, C. M. Soulette, T. P. Snutch, N. Loman, B. Paten, M. Loose, J. T. Simpson, H. E. Olsen, A. N. Brooks, M. Akeson, W. Timp, Nanopore native RNA sequencing of a human poly(A) transcriptome. *Nat. Methods*. **16**, 1297–1305 (2019).

34. D. Sapkota, A. M. Lake, W. Yang, C. Yang, H. Wesseling, A. Guise, C. Uncu, J. S. Dalal, A. W. Kraft, J.-M. Lee, M. S. Sands, J. A. Steen, J. D. Dougherty, Cell-Type-Specific Profiling of Alternative Translation Identifies Regulated Protein Isoform Variation in the Mouse Brain. *Cell Rep*. **26**, 594-607.e7 (2019).

35. J. L. Weirather, M. de Cesare, Y. Wang, P. Piazza, V. Sebastiano, X.-J. Wang, D. Buck, K. F. Au, Comprehensive comparison of Pacific Biosciences and Oxford Nanopore Technologies and their applications to transcriptome analysis. *F1000Res*. **6**, 100 (2017).

36. P. Wu, D. Zhou, W. Lin, Y. Li, H. Wei, X. Qian, Y. Jiang, F. He, Cell-type-resolved alternative splicing patterns in mouse liver. *DNA Res.* (2018), doi:10.1093/dnares/dsx055.

37. J.-R. Landry, D. L. Mager, B. T. Wilhelm, Complex controls: the role of alternative promoters in mammalian genomes. *Trends Genet.* **19**, 640–648 (2003).

38. G. A. C. Singer, J. Wu, P. Yan, C. Plass, T. H. M. Huang, R. V. Davuluri, Genome-wide analysis of alternative promoters of human genes using a custom promoter tiling array. *BMC Genomics*. **9**, 349 (2008).

39. L. Yu, E. Croze, K. D. Yamaguchi, T. Tran, A. T. Reder, V. Litvak, M. R. Volkert, Induction of a unique isoform of the NCOA7 oxidation resistance gene by interferon β-1b. *J. Interferon Cytokine Res.* **35**, 186–199 (2015).

40. Z. Pang, R. D. Junkins, R. Raudonis, A. J. MacNeil, C. McCormick, Z. Cheng, T.-J. Lin, Regulator of calcineurin 1 differentially regulates TLR-dependent MyD88 and TRIF signaling pathways. *PLoS ONE*. **13**, e0197491 (2018).

41. D. R. Garalde, E. A. Snell, D. Jachimowicz, B. Sipos, J. H. Lloyd, M. Bruce, N. Pantic, T. Admassu, P. James, A. Warland, M. Jordan, J. Ciccone, S. Serra, J. Keenan, S. Martin, L.

bioRxiv preprint doi: https://doi.org/10.1101/2020.07.06.190330; this version posted July 6, 2020. The copyright holder for this preprint (which was not certified by peer review) is the author/funder. All rights reserved. No reuse allowed without permission.

McNeill, E. J. Wallace, L. Jayasinghe, C. Wright, J. Blasco, S. Young, D. Brocklebank, S. Juul, J. Clarke, A. J. Heron, D. J. Turner, Highly parallel direct RNA sequencing on an array of nanopores. *Nat. Methods*. **15**, 201–206 (2018).

42. P.-H. Hsieh, Y.-J. Oyang, C.-Y. Chen, Effect of de novo transcriptome assembly on transcript quantification. *Sci Rep*. **9**, 8304 (2019).

43. M. O. Pollard, D. Gurdasani, A. J. Mentzer, T. Porter, M. S. Sandhu, Long reads: their purpose and place. *Hum. Mol. Genet.* **27**, R234–R241 (2018).

44. A. D. Tang, C. M. Soulette, M. J. van Baren, K. Hart, E. Hrabeta-Robinson, C. J. Wu, A. N. Brooks, "Full-length transcript characterization of *SF3B1* mutation in chronic lymphocytic leukemia reveals downregulation of retained introns" (preprint, Genomics, 2018), , doi:10.1101/410183.

45. M. K. Atianand, W. Hu, A. T. Satpathy, Y. Shen, E. P. Ricci, J. R. Alvarez-Dominguez, A. Bhatta, S. A. Schattgen, J. D. McGowan, J. Blin, J. E. Braun, P. Gandhi, M. J. Moore, H. Y. Chang, H. F. Lodish, D. R. Caffrey, K. A. Fitzgerald, A Long Noncoding RNA lincRNA-EPS Acts as a Transcriptional Brake to Restrain Inflammation. *Cell*. **165**, 1672–1685 (2016).

46. A.-J. Tong, X. Liu, B. J. Thomas, M. M. Lissner, M. R. Baker, M. D. Senagolage, A. L. Allred, G. D. Barish, S. T. Smale, A Stringent Systems Approach Uncovers Gene-Specific Mechanisms Regulating Inflammation. *Cell*. **165**, 165–179 (2016).

47. A. Frankish, M. Diekhans, A.-M. Ferreira, R. Johnson, I. Jungreis, J. Loveland, J. M. Mudge, C. Sisu, J. Wright, J. Armstrong, I. Barnes, A. Berry, A. Bignell, S. Carbonell Sala, J. Chrast, F. Cunningham, T. Di Domenico, S. Donaldson, I. T. Fiddes, C. García Girón, J. M. Gonzalez, T. Grego, M. Hardy, T. Hourlier, T. Hunt, O. G. Izuogu, J. Lagarde, F. J. Martin, L. Martínez, S. Mohanan, P. Muir, F. C. P. Navarro, A. Parker, B. Pei, F. Pozo, M. Ruffier, B. M. Schmitt, E. Stapleton, M.-M. Suner, I. Sycheva, B. Uszczynska-Ratajczak, J. Xu, A. Yates, D. Zerbino, Y. Zhang, B. Aken, J. S. Choudhary, M. Gerstein, R. Guigó, T. J. P. Hubbard, M. Kellis, B. Paten, A. Reymond, M. L. Tress, P. Flicek, GENCODE reference annotation for the human and mouse genomes. *Nucleic Acids Res.* **47**, D766–D773 (2019).

48. B. Wang, Q. Yin, AIM2 inflammasome activation and regulation: A structural perspective. *J. Struct. Biol.* **200**, 279–282 (2017).

49. M. T. Y. Lam, H. Cho, H. P. Lesch, D. Gosselin, S. Heinz, Y. Tanaka-Oishi, C. Benner, M. U. Kaikkonen, A. S. Kim, M. Kosaka, C. Y. Lee, A. Watt, T. R. Grossman, M. G. Rosenfeld, R. M. Evans, C. K. Glass, Rev-Erbs repress macrophage gene expression by inhibiting enhancer-directed transcription. *Nature*. **498**, 511–515 (2013).

bioRxiv preprint doi: https://doi.org/10.1101/2020.07.06.190330; this version posted July 6, 2020. The copyright holder for this preprint (which was not certified by peer review) is the author/funder. All rights reserved. No reuse allowed without permission.

50. D. Lara-Astiaso, A. Weiner, E. Lorenzo-Vivas, I. Zaretsky, D. A. Jaitin, E. David, H. Keren-Shaul, A. Mildner, D. Winter, S. Jung, N. Friedman, I. Amit, Immunogenetics. Chromatin state dynamics during blood formation. *Science*. **345**, 943–949 (2014).

51. D. W. Huang, B. T. Sherman, Q. Tan, J. R. Collins, W. G. Alvord, J. Roayaei, R. Stephens, M. W. Baseler, H. C. Lane, R. A. Lempicki, The DAVID Gene Functional Classification Tool: a novel biological module-centric algorithm to functionally analyze large gene lists. *Genome Biol.* **8**, R183 (2007).

52. S. D. Senanayake, D. A. Brian, Translation from the 5' untranslated region (UTR) of mRNA 1 is repressed, but that from the 5' UTR of mRNA 7 is stimulated in coronavirus-infected cells. *J. Virol.* **73**, 8003–8009 (1999).

53. T.-H. Chang, H.-Y. Huang, J. B.-K. Hsu, S.-L. Weng, J.-T. Horng, H.-D. Huang, An enhanced computational platform for investigating the roles of regulatory RNA and for identifying functional RNA motifs. *BMC Bioinformatics*. **14 Suppl 2**, S4 (2013).

54. A. R. Gruber, R. Lorenz, S. H. Bernhart, R. Neuböck, I. L. Hofacker, The Vienna RNA websuite. *Nucleic Acids Res.* **36**, W70-74 (2008).

55. T. A. Rouault, The role of iron regulatory proteins in mammalian iron homeostasis and disease. *Nat. Chem. Biol.* **2**, 406–414 (2006).

56. J. Wang, G. Chen, M. Muckenthaler, B. Galy, M. W. Hentze, K. Pantopoulos, Iron-mediated degradation of IRP2, an unexpected pathway involving a 2-oxoglutarate-dependent oxygenase activity. *Mol. Cell. Biol.* **24**, 954–965 (2004).

57. C. E. Outten, Checks and balances for the iron bank. *J. Biol. Chem.* **292**, 15990–15991 (2017).

58. S. Akira, S. Uematsu, O. Takeuchi, Pathogen recognition and innate immunity. *Cell*. **124**, 783–801 (2006).

59. R. Medzhitov, C. A. Janeway, Innate immune recognition and control of adaptive immune responses. *Semin. Immunol.* **10**, 351–353 (1998).

60. P. Carninci, A. Sandelin, B. Lenhard, S. Katayama, K. Shimokawa, J. Ponjavic, C. A. M. Semple, M. S. Taylor, P. G. Engström, M. C. Frith, A. R. R. Forrest, W. B. Alkema, S. L. Tan, C. Plessy, R. Kodzius, T. Ravasi, T. Kasukawa, S. Fukuda, M. Kanamori-Katayama, Y. Kitazume, H. Kawaji, C. Kai, M. Nakamura, H. Konno, K. Nakano, S. Mottagui-Tabar, P. Arner, A. Chesi, S. Gustincich, F. Persichetti, H. Suzuki, S. M. Grimmond, C. A. Wells, V. Orlando, C. Wahlestedt, E. T. Liu, M. Harbers, J. Kawai, V. B. Bajic, D. A. Hume, Y.

bioRxiv preprint doi: https://doi.org/10.1101/2020.07.06.190330; this version posted July 6, 2020. The copyright holder for this preprint (which was not certified by peer review) is the author/funder. All rights reserved. No reuse allowed without permission.

Hayashizaki, Genome-wide analysis of mammalian promoter architecture and evolution. *Nat. Genet.* **38**, 626–635 (2006).

61. B. Tian, J. L. Manley, Alternative polyadenylation of mRNA precursors. *Nat. Rev. Mol. Cell Biol.* **18**, 18–30 (2017).

62. E. T. Wang, R. Sandberg, S. Luo, I. Khrebtukova, L. Zhang, C. Mayr, S. F. Kingsmore, G. P. Schroth, C. B. Burge, Alternative isoform regulation in human tissue transcriptomes. *Nature*. **456**, 470–476 (2008).

63. C. Nishiyama, K. Takahashi, M. Nishiyama, K. Okumura, C. Ra, Y. Ohtake, T. Yokota, Splice isoforms of transcription factor Elf-1 affecting its regulatory function in transcription-molecular cloning of rat Elf-1. *Biosci. Biotechnol. Biochem.* **64**, 2601–2607 (2000).

64. J. Yang, W. Yang, N. Hirankarn, D. Q. Ye, Y. Zhang, H.-F. Pan, C. C. Mok, T. M. Chan, R. W. S. Wong, M. Y. Mok, K. W. Lee, S. N. Wong, A. M. H. Leung, X.-P. Li, Y. Avihingsanon, P. Rianthavorn, T. Deekajorndej, K. Suphapeetiporn, V. Shotelersuk, L. Baum, P. Kwan, T. L. Lee, M. H. K. Ho, P. P. W. Lee, W. H. S. Wong, S. Zeng, J. Zhang, C.-M. Wong, I. O. L. Ng, M.-M. Garcia-Barceló, S. S. Cherny, P. K.-H. Tam, P. C. Sham, C. S. Lau, Y. L. Lau, ELF1 is associated with systemic lupus erythematosus in Asian populations. *Hum. Mol. Genet.* **20**, 601–607 (2011).

65. Y. You, C. Zhou, D. Li, Z.-L. Cao, W. Shen, W.-Z. Li, S. Zhang, B. Hu, X. Shen, Sorting nexin 10 acting as a novel regulator of macrophage polarization mediates inflammatory response in experimental mouse colitis. *Sci Rep*. **6**, 20630 (2016).

66. Z. Qin, P. Stoilov, X. Zhang, Y. Xing, SEASTAR: systematic evaluation of alternative transcription start sites in RNA. *Nucleic Acids Res.* **46**, e45 (2018).

67. J. Liu, E. Shue, K. L. Ewalt, P. Schimmel, A new gamma-interferon-inducible promoter and splice variants of an anti-angiogenic human tRNA synthetase. *Nucleic Acids Res.* **32**, 719–727 (2004).

68. M. Miyanokoshi, T. Tanaka, M. Tamai, Y. Tagawa, K. Wakasugi, Expression of the rodent-specific alternative splice variant of tryptophanyl-tRNA synthetase in murine tissues and cells. *Sci Rep*. **3**, 3477 (2013).

69. J. R. Kulzer, M. L. Stitzel, M. A. Morken, J. R. Huyghe, C. Fuchsberger, J. Kuusisto, M. Laakso, M. Boehnke, F. S. Collins, K. L. Mohlke, A common functional regulatory variant at a type 2 diabetes locus upregulates ARAP1 expression in the pancreatic beta cell. *Am. J. Hum. Genet.* **94**, 186–197 (2014).

bioRxiv preprint doi: https://doi.org/10.1101/2020.07.06.190330; this version posted July 6, 2020. The copyright holder for this preprint (which was not certified by peer review) is the author/funder. All rights reserved. No reuse allowed without permission.

70. K. Kawakubo, C. E. Samuel, Human RNA-specific adenosine deaminase (ADAR1) gene specifies transcripts that initiate from a constitutively active alternative promoter. *Gene*. **258**, 165–172 (2000).

71. S. Lykke-Andersen, S. Piñol-Roma, J. Kjems, Alternative splicing of the ADAR1 transcript in a region that functions either as a 5'-UTR or an ORF. *RNA*. **13**, 1732–1744 (2007).

72. M. F. Arteaga, D. Alvarez de la Rosa, J. A. Alvarez, C. M. Canessa, Multiple translational isoforms give functional specificity to serum- and glucocorticoid-induced kinase 1. *Mol. Biol. Cell*. **18**, 2072–2080 (2007).

73. T. Kobayashi, M. Deak, N. Morrice, P. Cohen, Characterization of the structure and regulation of two novel isoforms of serum- and glucocorticoid-induced protein kinase. *Biochem. J.* **344 Pt 1**, 189–197 (1999).

74. F. Lang, C. Böhmer, M. Palmada, G. Seebohm, N. Strutz-Seebohm, V. Vallon, (Patho)physiological significance of the serum- and glucocorticoid-inducible kinase isoforms. *Physiol. Rev.* **86**, 1151–1178 (2006).

75. R. W. Johnstone, J. A. Trapani, Transcription and growth regulatory functions of the HIN-200 family of proteins. *Mol. Cell. Biol.* **19**, 5833–5838 (1999).

76. T. Bürckstümmer, C. Baumann, S. Blüml, E. Dixit, G. Dürnberger, H. Jahn, M. Planyavsky, M. Bilban, J. Colinge, K. L. Bennett, G. Superti-Furga, An orthogonal proteomic-genomic screen identifies AIM2 as a cytoplasmic DNA sensor for the inflammasome. *Nat. Immunol.* **10**, 266–272 (2009).

77. T. Fernandes-Alnemri, J.-W. Yu, P. Datta, J. Wu, E. S. Alnemri, AIM2 activates the inflammasome and cell death in response to cytoplasmic DNA. *Nature*. **458**, 509–513 (2009).

78. V. Hornung, A. Ablasser, M. Charrel-Dennis, F. Bauernfeind, G. Horvath, D. R. Caffrey, E. Latz, K. A. Fitzgerald, AIM2 recognizes cytosolic dsDNA and forms a caspase-1-activating inflammasome with ASC. *Nature*. **458**, 514–518 (2009).

79. F. Mignone, C. Gissi, S. Liuni, G. Pesole, Untranslated regions of mRNAs. *Genome Biol.* **3**, REVIEWS0004 (2002).

80. A. W. van der Velden, A. A. Thomas, The role of the 5' untranslated region of an mRNA in translation regulation during development. *Int. J. Biochem. Cell Biol.* **31**, 87–106 (1999).

81. R. P. Jansen, mRNA localization: message on the move. *Nat. Rev. Mol. Cell Biol.* **2**, 247–256 (2001).

bioRxiv preprint doi: https://doi.org/10.1101/2020.07.06.190330; this version posted July 6, 2020. The copyright holder for this preprint (which was not certified by peer review) is the author/funder. All rights reserved. No reuse allowed without permission.

82. A. Bashirullah, R. L. Cooperstock, H. D. Lipshitz, Spatial and temporal control of RNA stability. *Proc. Natl. Acad. Sci. U.S.A.* **98**, 7025–7028 (2001).

83. P. J. Leedman, A. R. Stein, W. W. Chin, J. T. Rogers, Thyroid hormone modulates the interaction between iron regulatory proteins and the ferritin mRNA iron-responsive element. *J. Biol. Chem.* **271**, 12017–12023 (1996).

84. D. D. Crane, T. J. Bauler, T. D. Wehrly, C. M. Bosio, Mitochondrial ROS potentiates indirect activation of the AIM2 inflammasome. *Front Microbiol*. **5**, 438 (2014).

85. E. S. Hanson, E. A. Leibold, Regulation of the iron regulatory proteins by reactive nitrogen and oxygen species. *Gene Expr.* **7**, 367–376 (1999).

86. C. Li, Y. Zhang, X. Cheng, H. Yuan, S. Zhu, J. Liu, Q. Wen, Y. Xie, J. Liu, G. Kroemer, D. J. Klionsky, M. T. Lotze, H. J. Zeh, R. Kang, D. Tang, PINK1 and PARK2 Suppress Pancreatic Tumorigenesis through Control of Mitochondrial Iron-Mediated Immunometabolism. *Dev. Cell*. **46**, 441-455.e8 (2018).

87. A. H. Corbett, Post-transcriptional regulation of gene expression and human disease. *Curr. Opin. Cell Biol.* **52**, 96–104 (2018).

88. W. Zhang, Y. Cai, W. Xu, Z. Yin, X. Gao, S. Xiong, AIM2 facilitates the apoptotic DNA-induced systemic lupus erythematosus via arbitrating macrophage functional maturation. *J. Clin. Immunol.* **33**, 925–937 (2013).

89. K. Vanarsa, Y. Ye, J. Han, C. Xie, C. Mohan, T. Wu, Inflammation associated anemia and ferritin as disease markers in SLE. *Arthritis Res. Ther.* **14**, R182 (2012).

90. J. Schindelin, I. Arganda-Carreras, E. Frise, V. Kaynig, M. Longair, T. Pietzsch, S. Preibisch, C. Rueden, S. Saalfeld, B. Schmid, J.-Y. Tinevez, D. J. White, V. Hartenstein, K. Eliceiri, P. Tomancak, A. Cardona, Fiji: an open-source platform for biological-image analysis. *Nat. Methods*. **9**, 676–682 (2012).

91. C. Trapnell, L. Pachter, S. L. Salzberg, TopHat: discovering splice junctions with RNA-Seq. *Bioinformatics*. **25**, 1105–1111 (2009).

92. S. Anders, W. Huber, Differential expression analysis for sequence count data. *Genome Biol.* **11**, R106 (2010).

93. R. E. Workman, A. D. Tang, P. S. Tang, M. Jain, J. R. Tyson, R. Razaghi, P. C. Zuzarte, T. Gilpatrick, A. Payne, J. Quick, N. Sadowski, N. Holmes, J. G. de Jesus, K. L. Jones, C. M. Soulette, T. P. Snutch, N. Loman, B. Paten, M. Loose, J. T. Simpson, H. E. Olsen, A. N.

bioRxiv preprint doi: https://doi.org/10.1101/2020.07.06.190330; this version posted July 6, 2020. The copyright holder for this preprint (which was not certified by peer review) is the author/funder. All rights reserved. No reuse allowed without permission.

Brooks, M. Akeson, W. Timp, Nanopore native RNA sequencing of a human poly(A) transcriptome. *Nat Methods*. **16**, 1297–1305 (2019).

94. H. Li, Minimap and miniasm: fast mapping and de novo assembly for noisy long sequences. *Bioinformatics*. **32**, 2103–2110 (2016).

95. H. Li, B. Handsaker, A. Wysoker, T. Fennell, J. Ruan, N. Homer, G. Marth, G. Abecasis, R. Durbin, 1000 Genome Project Data Processing Subgroup, The Sequence Alignment/Map format and SAMtools. *Bioinformatics*. **25**, 2078–2079 (2009).

96. B. Langmead, S. L. Salzberg, Fast gapped-read alignment with Bowtie 2. *Nat. Methods*. **9**, 357–359 (2012).

97. D. Kim, G. Pertea, C. Trapnell, H. Pimentel, R. Kelley, S. L. Salzberg, TopHat2: accurate alignment of transcriptomes in the presence of insertions, deletions and gene fusions. *Genome Biol.* **14**, R36 (2013).

98. A. N. Brooks, L. Yang, M. O. Duff, K. D. Hansen, J. W. Park, S. Dudoit, S. E. Brenner, B. R. Graveley, Conservation of an RNA regulatory map between Drosophila and mammals. *Genome Res.* **21**, 193–202 (2011).

99. A. Frankish, M. Diekhans, A.-M. Ferreira, R. Johnson, I. Jungreis, J. Loveland, J. M. Mudge, C. Sisu, J. Wright, J. Armstrong, I. Barnes, A. Berry, A. Bignell, S. Carbonell Sala, J. Chrast, F. Cunningham, T. Di Domenico, S. Donaldson, I. T. Fiddes, C. García Girón, J. M. Gonzalez, T. Grego, M. Hardy, T. Hourlier, T. Hunt, O. G. Izuogu, J. Lagarde, F. J. Martin, L. Martínez, S. Mohanan, P. Muir, F. C. P. Navarro, A. Parker, B. Pei, F. Pozo, M. Ruffier, B. M. Schmitt, E. Stapleton, M.-M. Suner, I. Sycheva, B. Uszczynska-Ratajczak, J. Xu, A. Yates, D. Zerbino, Y. Zhang, B. Aken, J. S. Choudhary, M. Gerstein, R. Guigó, T. J. P. Hubbard, M. Kellis, B. Paten, A. Reymond, M. L. Tress, P. Flicek, GENCODE reference annotation for the human and mouse genomes. *Nucleic Acids Res.* **47**, D766–D773 (2019).

100. A. D. Tang, C. M. Soulette, M. J. van Baren, K. Hart, E. Hrabeta-Robinson, C. J. Wu, A. N. Brooks, "Full-length transcript characterization of *SF3B1* mutation in chronic lymphocytic leukemia reveals downregulation of retained introns" (preprint, Genomics, 2018), , doi:10.1101/410183.

101. M. K. Atianand, W. Hu, A. T. Satpathy, Y. Shen, E. P. Ricci, J. R. Alvarez-Dominguez, A. Bhatta, S. A. Schattgen, J. D. McGowan, J. Blin, J. E. Braun, P. Gandhi, M. J. Moore, H. Y. Chang, H. F. Lodish, D. R. Caffrey, K. A. Fitzgerald, A Long Noncoding RNA lincRNA-EPS Acts as a Transcriptional Brake to Restrain Inflammation. *Cell*. **165**, 1672–1685 (2016).

bioRxiv preprint doi: https://doi.org/10.1101/2020.07.06.190330; this version posted July 6, 2020. The copyright holder for this preprint (which was not certified by peer review) is the author/funder. All rights reserved. No reuse allowed without permission.

102. A.-J. Tong, X. Liu, B. J. Thomas, M. M. Lissner, M. R. Baker, M. D. Senagolage, A. L. Allred, G. D. Barish, S. T. Smale, A Stringent Systems Approach Uncovers Gene-Specific Mechanisms Regulating Inflammation. *Cell*. **165**, 165–179 (2016).

103. A. S. Hinrichs, D. Karolchik, R. Baertsch, G. P. Barber, G. Bejerano, H. Clawson, M. Diekhans, T. S. Furey, R. A. Harte, F. Hsu, J. Hillman-Jackson, R. M. Kuhn, J. S. Pedersen, A. Pohl, B. J. Raney, K. R. Rosenbloom, A. Siepel, K. E. Smith, C. W. Sugnet, A. Sultan-Qurraie, D. J. Thomas, H. Trumbower, R. J. Weber, M. Weirauch, A. S. Zweig, D. Haussler, W. J. Kent, The UCSC Genome Browser Database: update 2006. *Nucleic Acids Res.* **34**, D590-598 (2006).

104. M. Nowicka, M. D. Robinson, DRIMSeq: a Dirichlet-multinomial framework for multivariate count outcomes in genomics. *F1000Res*. **5**, 1356 (2016).

105. C. Trapnell, B. A. Williams, G. Pertea, A. Mortazavi, G. Kwan, M. J. van Baren, S. L. Salzberg, B. J. Wold, L. Pachter, Transcript assembly and quantification by RNA-Seq reveals unannotated transcripts and isoform switching during cell differentiation. *Nat. Biotechnol.* **28**, 511–515 (2010).

106. M. I. Love, W. Huber, S. Anders, Moderated estimation of fold change and dispersion for RNA-seq data with DESeq2. *Genome Biol.* **15**, 550 (2014).

107. H. Wickham, *ggplot2* (Springer New York, New York, NY, 2009; http://link.springer.com/10.1007/978-0-387-98141-3).

108. T. Hulsen, J. de Vlieg, W. Alkema, BioVenn - a web application for the comparison and visualization of biological lists using area-proportional Venn diagrams. *BMC Genomics*. **9**, 488 (2008).

109. A. R. Quinlan, I. M. Hall, BEDTools: a flexible suite of utilities for comparing genomic features. *Bioinformatics*. **26**, 841–842 (2010).

110. S. Anders, P. T. Pyl, W. Huber, HTSeq--a Python framework to work with high-throughput sequencing data. *Bioinformatics*. **31**, 166–169 (2015).

111. S. Heinz, C. Benner, N. Spann, E. Bertolino, Y. C. Lin, P. Laslo, J. X. Cheng, C. Murre, H. Singh, C. K. Glass, Simple combinations of lineage-determining transcription factors prime cis-regulatory elements required for macrophage and B cell identities. *Mol. Cell*. **38**, 576–589 (2010).

bioRxiv preprint doi: https://doi.org/10.1101/2020.07.06.190330; this version posted July 6, 2020. The copyright holder for this preprint (which was not certified by peer review) is the author/funder. All rights reserved. No reuse allowed without permission.

Figure 1

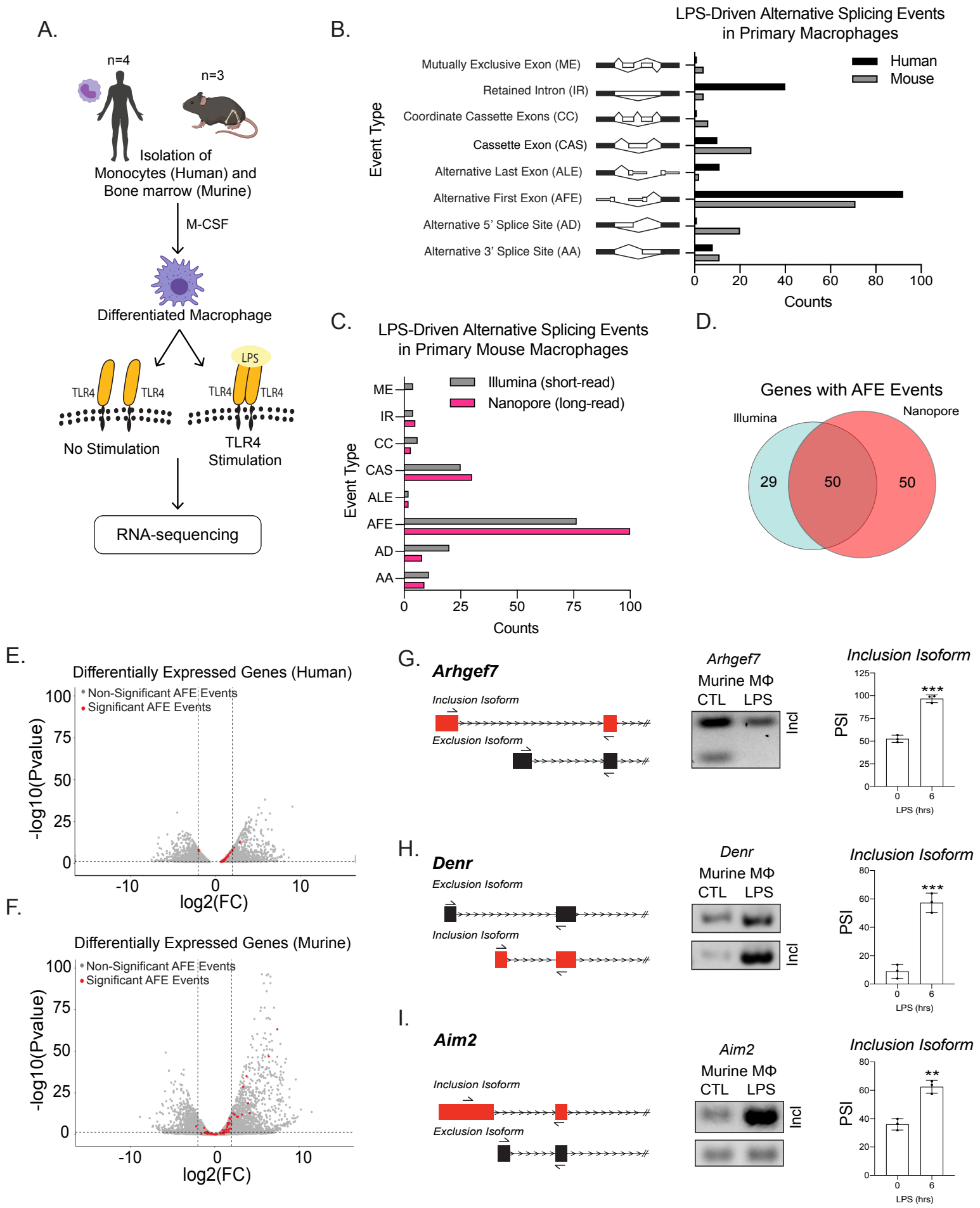

Figure 2

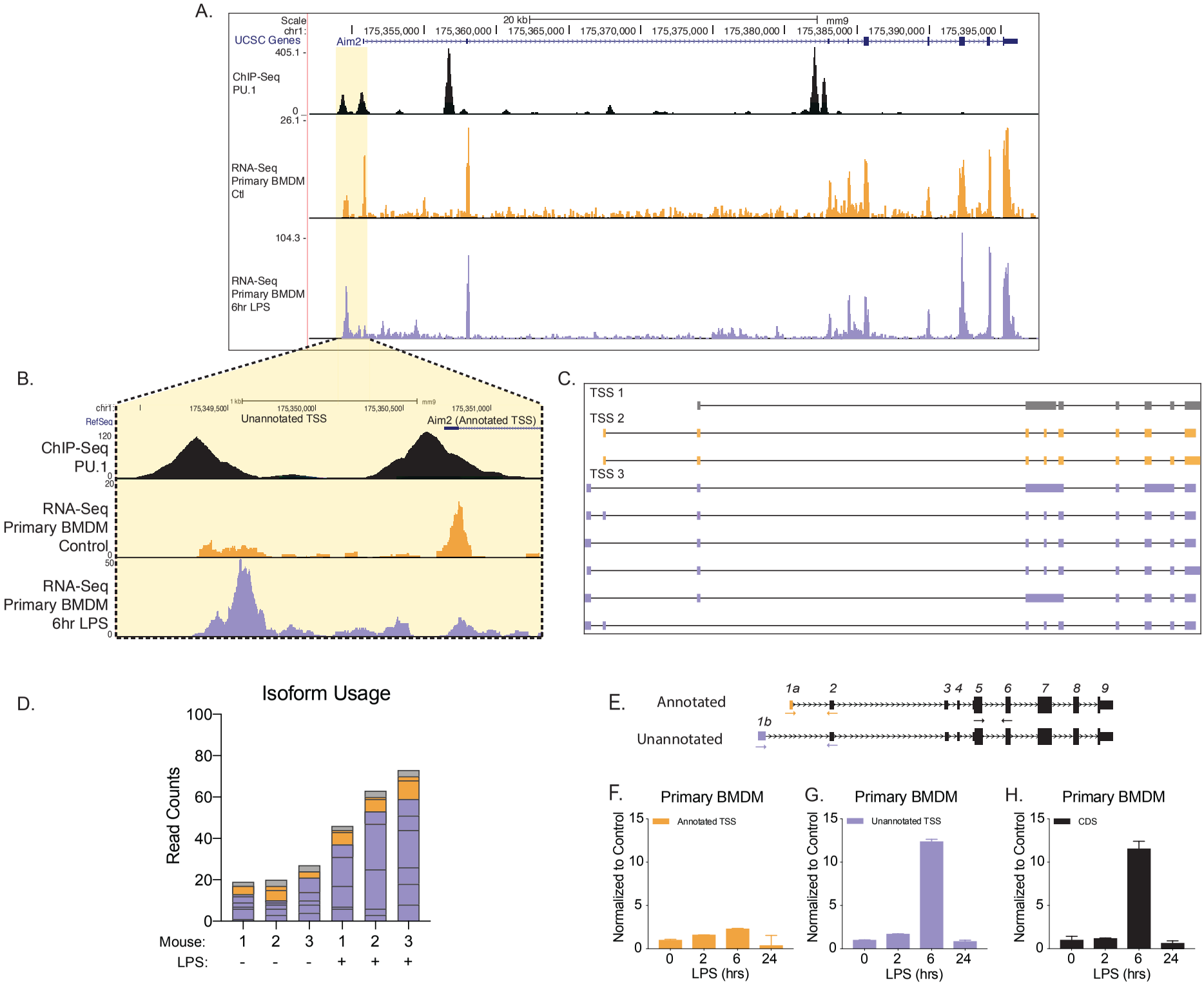

bioRxiv preprint doi: https://doi.org/10.1101/2020.07.06.190330; this version posted July 6, 2020. The copyright holder for this preprint (which was not certified by peer review) is the author/funder. All rights reserved. No reuse allowed without permission.

bioRxiv preprint doi: https://doi.org/10.1101/2020.07.06.190330; this version posted July 6, 2020. The copyright holder for this preprint (which was not certified by peer review) is the author/funder. All rights reserved. No reuse allowed without permission.

Figure 3

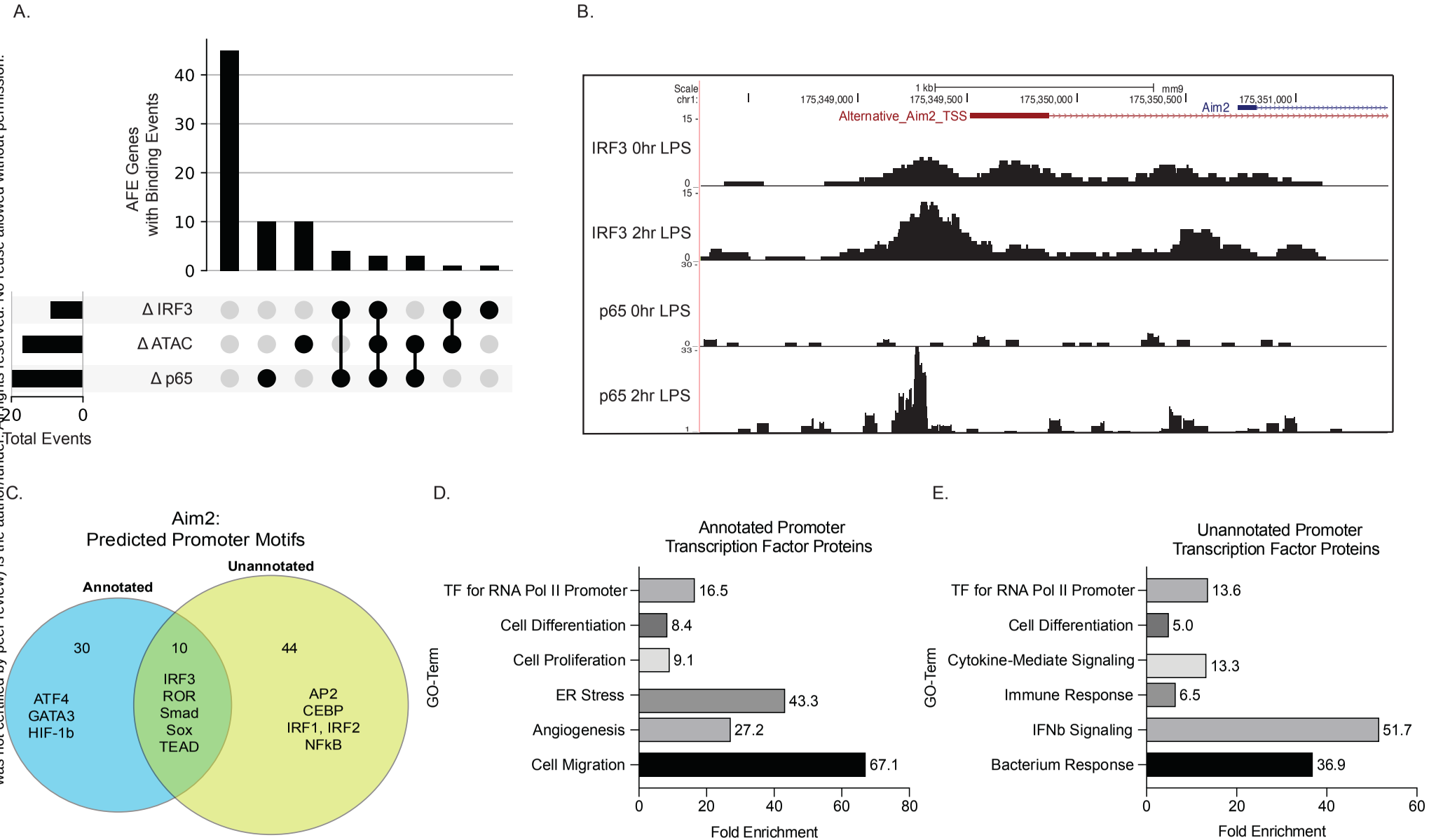

bioRxiv preprint doi: https://doi.org/10.1101/2020.07.06.190330; this version posted July 6, 2020. The copyright holder for this preprint (which was not certified by peer review) is the author/funder. All rights reserved. No reuse allowed without permission.

Figure 4

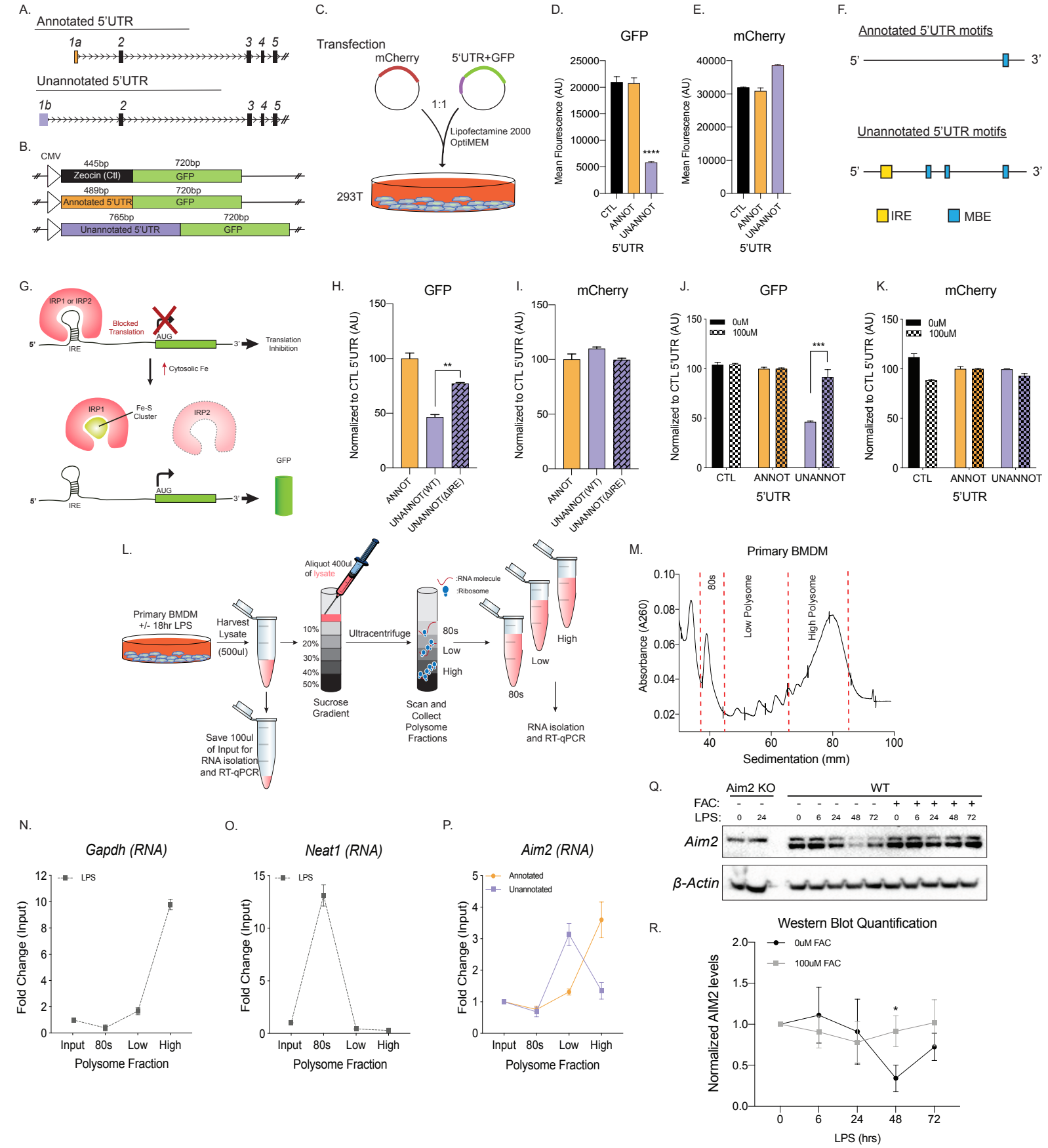

bioRxiv preprint doi: https://doi.org/10.1101/2020.07.06.190330; this version posted July 6, 2020. The copyright holder for this preprint (which was not certified by peer review) is the author/funder. All rights reserved. No reuse allowed without permission.

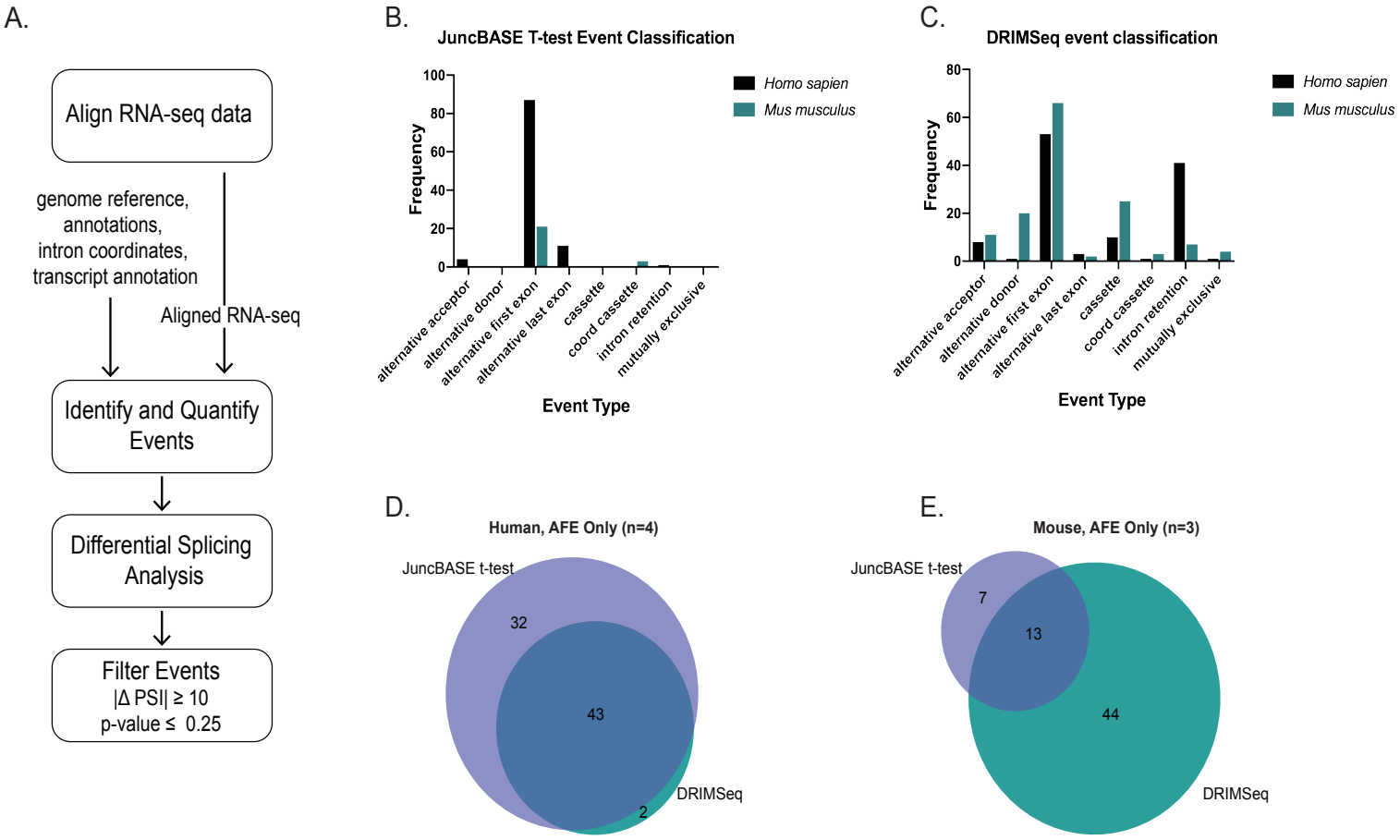

Supplemental Fig 1: Computational Pipeline and comparison of t-test and DRIMSeq alternative splicing events. (A) Bioinformatic pipeline for Human and Mouse RNA-seq data. (B) Alternative splicing event type classification of significant differential splicing events ($|\Delta PSI| \geq 10$ and corrected p-value ≤ 0.25) in Human and Mouse macrophages +/- LPS as identified and quantified using the t-test with JuncBASE. The AFE event is the most predominant in both human and mouse samples. (C) AS splicing event type classification of significant differential splicing events ($|\Delta PSI| \geq 10$ and corrected p-value ≤ 0.25) in human and mouse macrophages +/- LPS as quantified using the Dirichlet-multinomial framework applied by DRIMSeq. The AFE event is the most predominant in both human and mouse samples. (D)A comparison of genes found to have significant AFE events following +/- LPS stimulation of Human monocyte-derived macrophage cells by the JuncBASE t-test and DRIMSeq. There were 32 genes unique to the analysis that applied the JuncBASE t-test, 2 genes unique to the analysis that applied DRIMSeq, and 43 genes in common between the two sets of analyses. (E) A comparison of genes found to have significant AFE events following +/- LPS stimulation of Mouse bone marrow-derived macrophage cells by the JuncBASE t-test and DRIMSeq. There were 7 genes unique to the analysis that applied the JuncBASE t-test, 44 genes unique to the analysis that applied DRIMSeq, and 13 genes in common between the two sets of analyses.

bioRxiv preprint doi: https://doi.org/10.1101/2020.07.06.190330; this version posted July 6, 2020. The copyright holder for this preprint (which was not certified by peer review) is the author/funder. All rights reserved. No reuse allowed without permission.

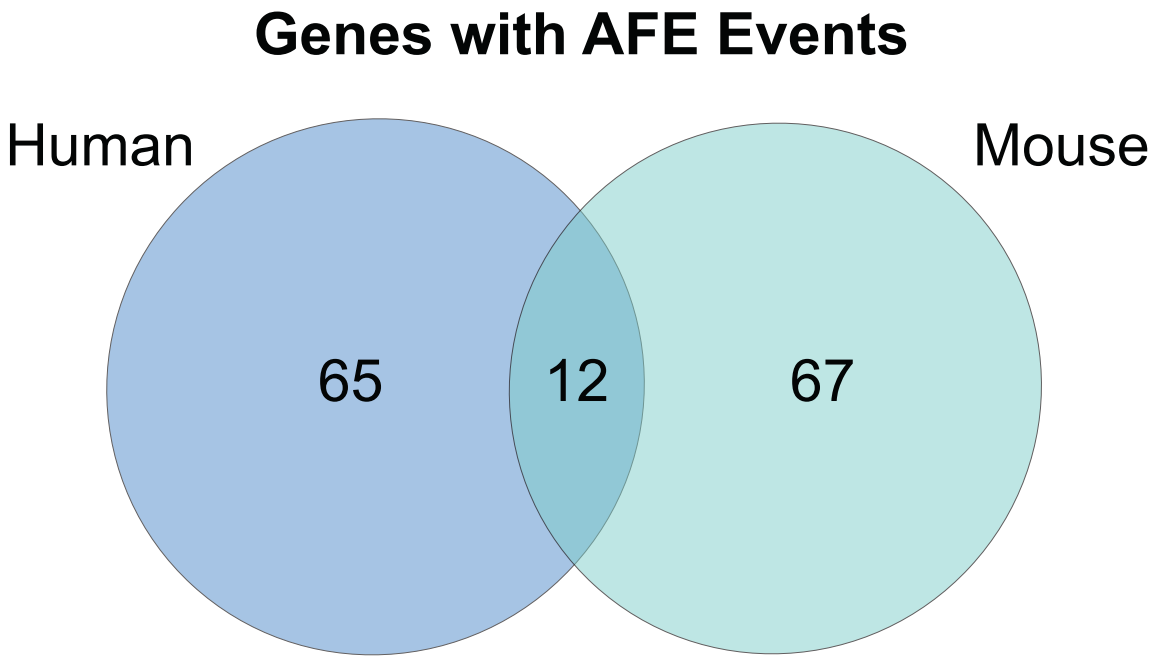

Supplemental Fig. 2: AFE conservation in mouse and human. Venn diagram denoting unique and overlapping genes with significant alternative first exon (AFE) switches in human and mouse.

bioRxiv preprint doi: https://doi.org/10.1101/2020.07.06.190330; this version posted July 6, 2020. The copyright holder for this preprint (which was not certified by peer review) is the author/funder. All rights reserved. No reuse allowed without permission.

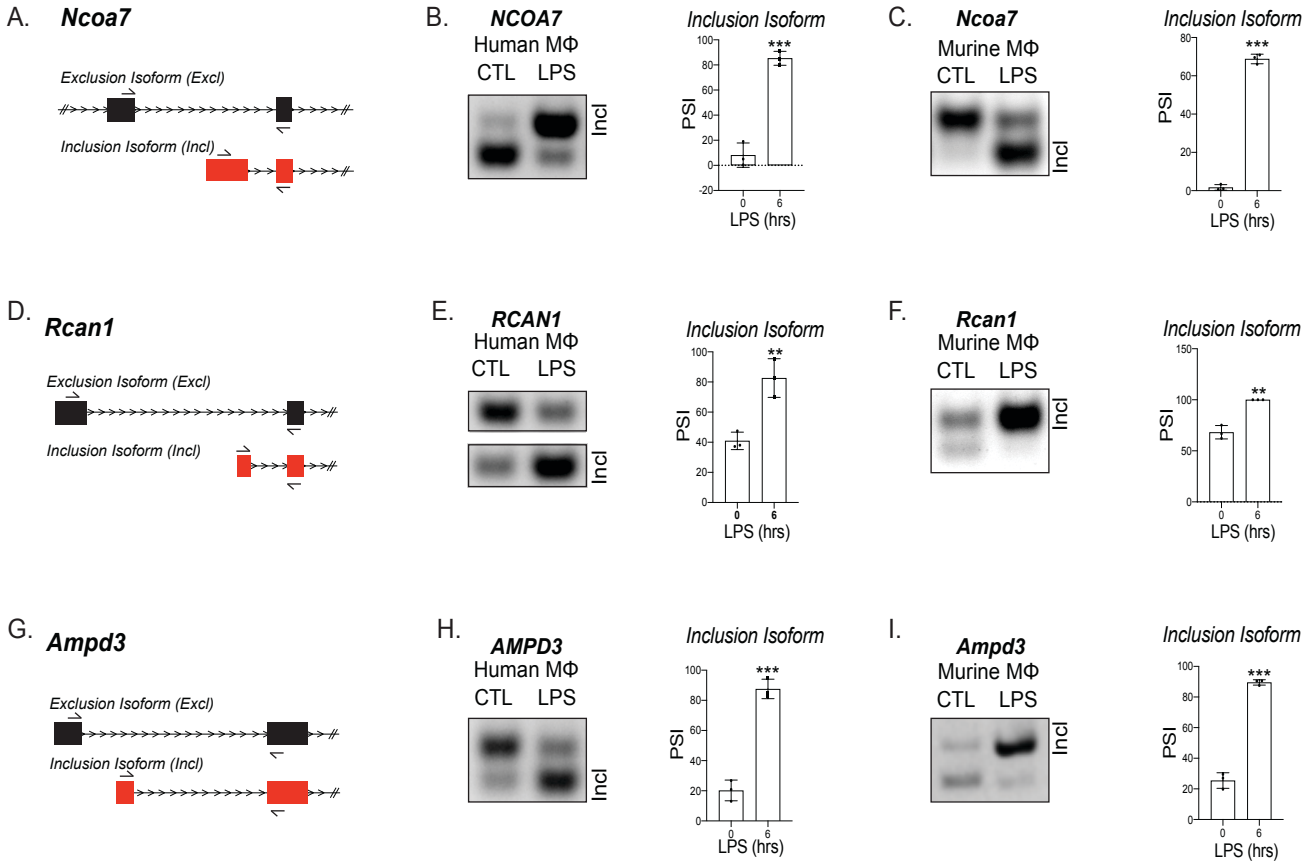

Supplemental Fig. 3: Validation of mouse and human alternative first exon events. (A) mRNA transcript diagram of the exclusion and inclusion isoform of Ncoa7 for human and murine macrophages. RT-PCR of human (B) and murine (C) macorphages, Rcan1 (D-F) and Ampd3 (G-I) with PSI calculation.

bioRxiv preprint doi: https://doi.org/10.1101/2020.07.06.190330; this version posted July 6, 2020. The copyright holder for this preprint (which was not certified by peer review) is the author/funder. All rights reserved. No reuse allowed without permission.

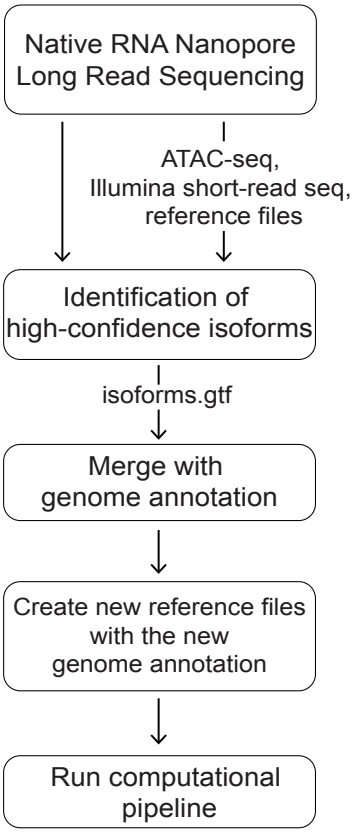

Supplemental Fig. 4: Bioinformatic pipeline. Schematic describing the steps taken to analyze alternative splicing of native RNA nanopore sequencing.

bioRxiv preprint doi: https://doi.org/10.1101/2020.07.06.190330; this version posted July 6, 2020. The copyright holder for this preprint (which was not certified by peer review) is the author/funder. All rights reserved. No reuse allowed without permission.

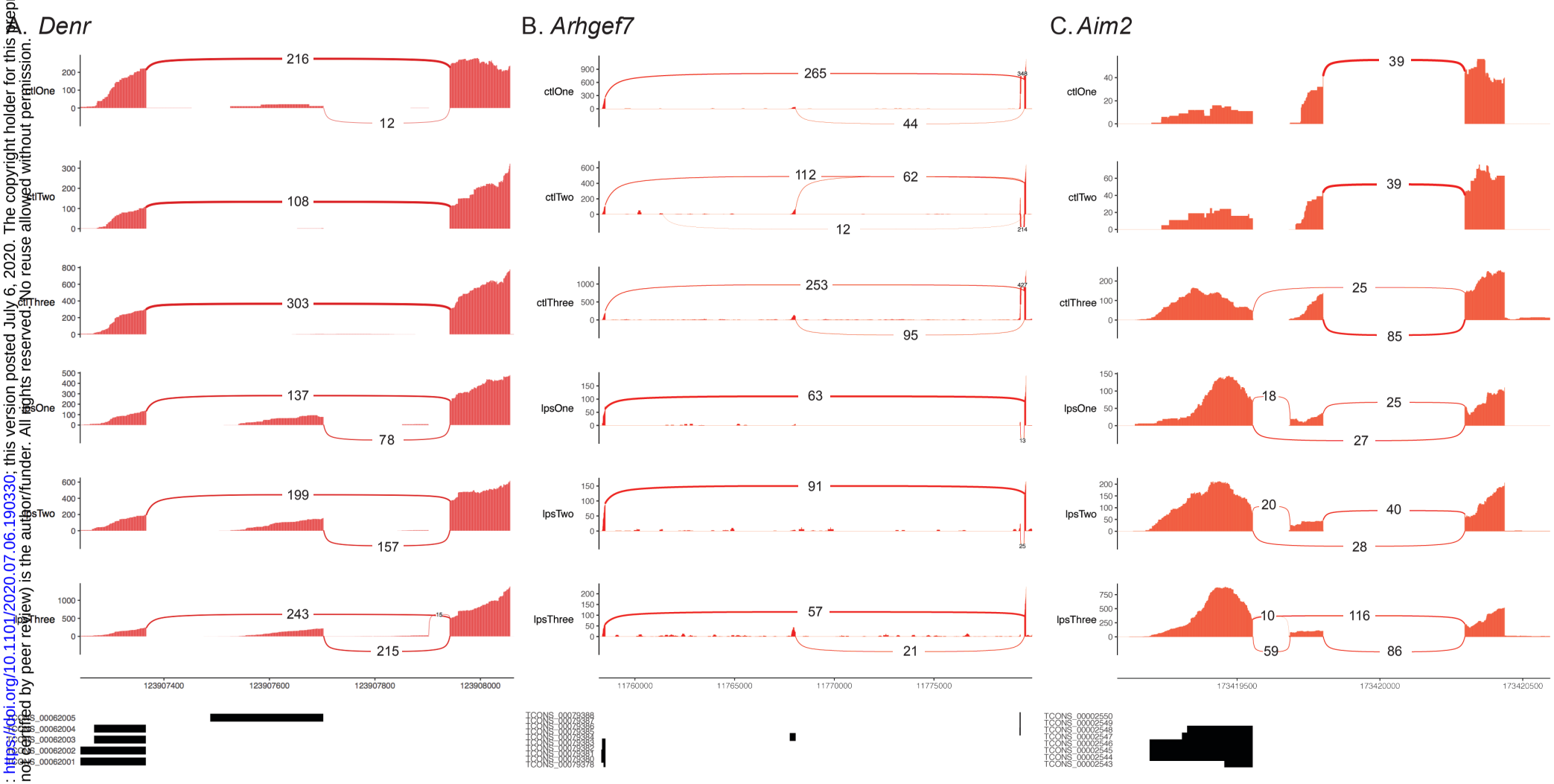

Supplemental Fig. 5: Validated unannotated alternative first exon isoforms. Sashimi plots showing AFE usage in (A) Denr, (B) Arhgef7, and (C) Aim2 involving novel isoforms identified using nanopore sequencing.

bioRxiv preprint doi: https://doi.org/10.1101/2020.07.06.190330; this version posted July 6, 2020. The copyright holder for this preprint (which was not certified by peer review) is the author/funder. All rights reserved. No reuse allowed without permission.

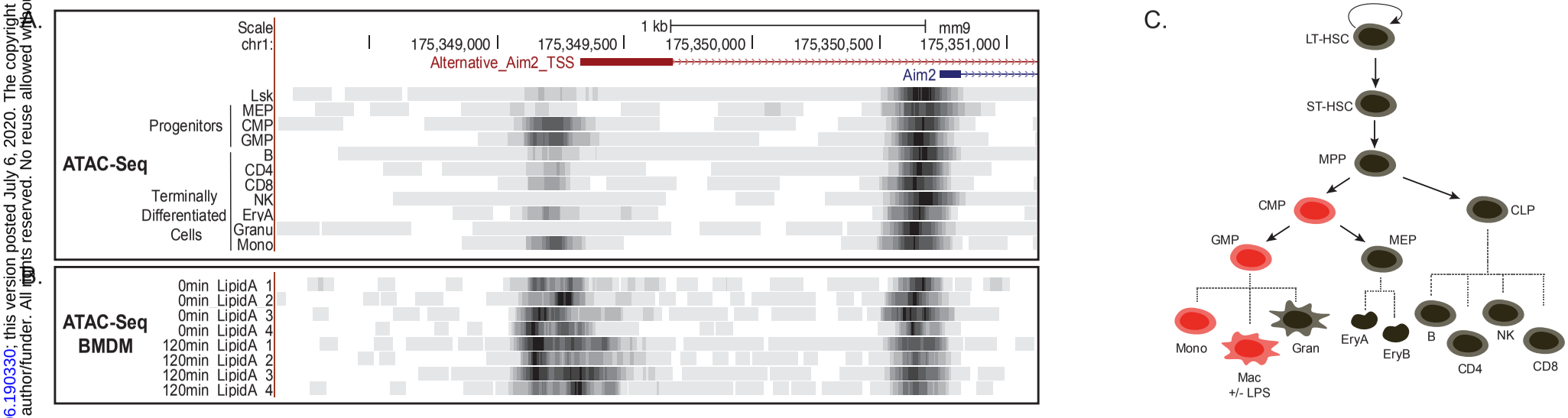

Supplemental Fig 6: Chromatin remodeling not a mechanism driving novel Aim2 isoform. (A) mm9 genome browser shot between chr1:175,348,283-175,351,422 indicating ATAC-seq of cells from hematopoietic tree. (B) mm9 genome browser shot between chr1:175,348,283-175,351,422 indicating ATAC-seq of BMDMs +/- Lipid A for 2 hrs. (C) Schematic summarizing promoter accessibility of novel Aim2 isoform, red=accessible and black=not accessible.

bioRxiv preprint doi: https://doi.org/10.1101/2020.07.06.190330; this version posted July 6, 2020. The copyright holder for this preprint (which was not certified by peer review) is the author/funder. All rights reserved. No reuse allowed without permission.

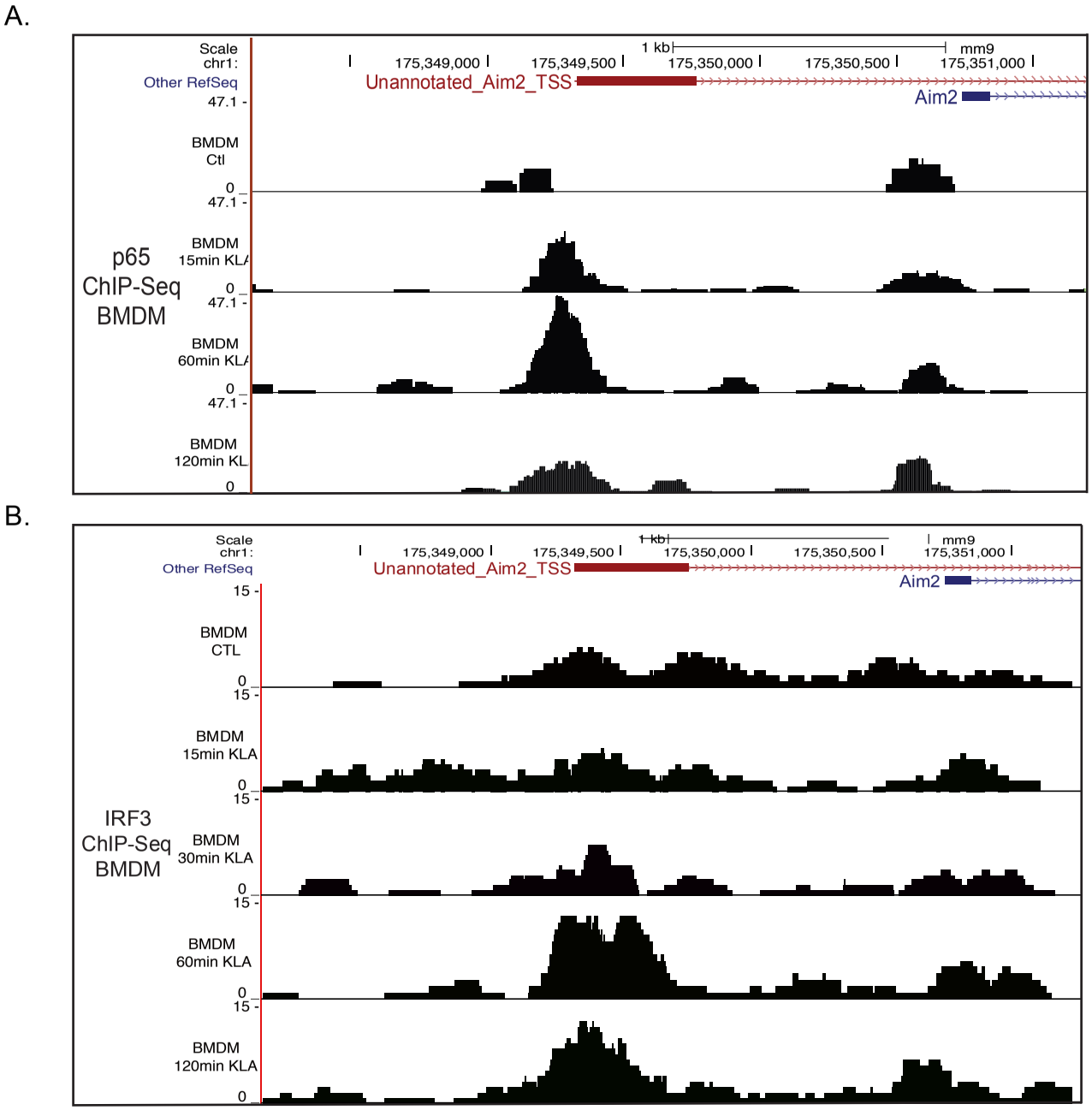

Supplemental Fig 7: Novel Aim2 isoform driven by IRF3 and p65 transcription factors. mm9 genome browser shot between chr1:175,348,283-175,351,422 for ChIP-seq of p65 binding (A) and IRF3 binding (B).

bioRxiv preprint doi: https://doi.org/10.1101/2020.07.06.190330; this version posted July 6, 2020. The copyright holder for this preprint (which was not certified by peer review) is the author/funder. All rights reserved. No reuse allowed without permission.

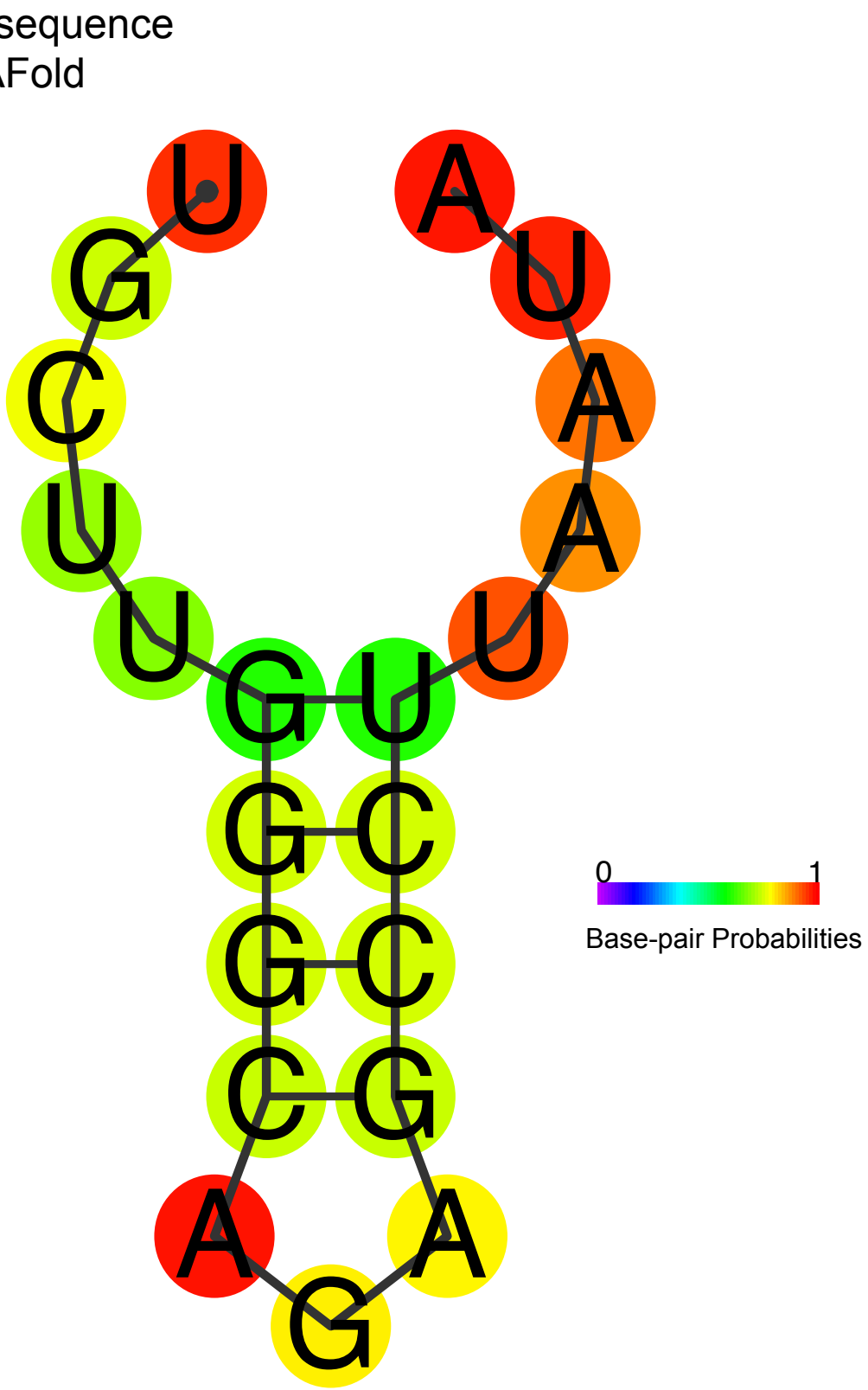

Supplemental Fig 8: IRE hairpin structure predicted. Using the Vienna RNAFold package, the IRE motif is folded into a hairpin, with strong base-pairing.